

Doctor thesis

Synthesis of novel π -conjugated oligomers and D-A type copolymers for optoelectronic applications

(光電子デバイスへの応用を目指した π -共役オリゴ
マーおよび D-A 型コポリマーの合成)

Zhifang Tan

Graduate school of Engineering,

Hiroshima University

March, 2014

Contents

Chapter 1. General Introduction	-----	1
1.1 Background	-----	1
1.2 Principle of polymer solar cells with bulk heterojunction structure	--	11
1.3 The aim of the present work	-----	16
1.4 References	-----	19
Chapter 2. Synthesis and Photovoltaic Applications of Main-chain Type Polymers with Benzodithiophene and Bisthienylacrylonitrile Units	----	23
2.1 Introduction	-----	23
2.2 Experimental	-----	25
2.3 Results and discussion	-----	33
2.3.1 Synthesis and characterization	-----	33
2.3.2 Thermal properties	-----	34
2.3.3 Optical properties	-----	36
2.3.4 Electrochemical properties	-----	37
2.3.5 Photovoltaic properties	-----	40
2.4 Conclusions	-----	43
2.5 References	-----	45
Chapter 3. Effects of π-conjugated side chains on properties and performances of photovoltaic copolymers	-----	48

3.1	Introduction	-----	48
3.2	Experimental	-----	50
3.3	Results and discussion	-----	57
3.3.1	Synthesis and characterization	-----	57
3.3.2	Thermal properties	-----	58
3.3.3	Optical properties	-----	60
3.3.4	Electrochemical properties	-----	62
3.3.5	Photovoltaic properties	-----	64
3.4	Conclusions	-----	68
3.5	References	-----	70

Chapter 4. Synthesis and electrical properties of novel oligothiophenes partially containing 3,4-ethylenedioxythiophenes ----- 73

4.1	Introduction	-----	73
4.2	Experimental	-----	74
4.3	Results and discussion	-----	82
4.3.1	Synthesis of hybrid EDOT-containing oligothiophenes	-----	82
4.3.2	Geometrical effect of EDOT	-----	82
4.3.3	Optical properties on <i>EnTs</i>	-----	84
4.3.4	Electrochemical stabilities of <i>EnTs</i>	-----	86
4.3.5	Film forming property	-----	87
4.3.6	Electrical properties of solid-state E11T	-----	88
4.4	Conclusions	-----	93
4.5	References	-----	94

Chapter 5. Summary	-----	98
Acknowledgement	-----	100
List of the related publications	-----	102

Chapter 1

General Introduction

1.1 Background

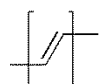
1.1.1 History and types

In 1862, a partly conductive material was obtained by oxidating aniline in sulfuric acid by Henry Letheby, probably as same as polyaniline.^[1,2] The conductive organic materials (COMs) firstly arose in the field of materials science. The study of dark/photo-conductivity of anthracene crystals was reported in early 20th century. Afterward, many researchers paid attentions to this topic. However, such studies did not give rise to further development. In the 1950s, researchers discovered that polycyclic aromatic compounds could form semiconducting charge-transfer complex salts with halogens, for example, perylene-iodine complex with conductivity of 0.12 S/cm.^[3] This result also indicated that organic compounds could carry current. Later, in the 1960s,^[4,5] molecular crystals were investigated intensively because of discovery of electroluminescence. Moreover, in 1977, conducting polymers, halogen derivatives of polyacetylene, were reported by Heeger, Shirakawa and MacDiarmid with oxidizing and iodine-doping treatment.^[6,7] On the basis of this research, they received the Nobel Prize in Chemistry for "The discovery and development of conductive polymers" in

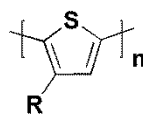
2000.^[8] Since then, the research of COMs has developed energetically. Not only the synthesis of COMs, the characterization and processing were also developed owing to the large efforts of both academic and industrial research laboratories.

It is now well-known that the COMs can be defined as an organic material with semiconductor properties, that is, with an electrical conductivity between that of insulators and that of metals.

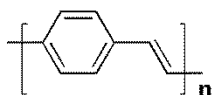
There are many different types of COMs,^[9] they include polymers with conjugated bonds, such as poly(3-alkylthiophene) and polycarbazole, and poly(p-phenylene vinylene), as well as polyacetylene and its derivatives; oligomers with conjugated system, such as oligothiophene, oligopyrrole; aromatic compounds, such as fullerene, pentacene, graphene, naphthalene, anthracene, and violanthrene; natural pigments, such as phthalocyanines, chlorophyll and β -carotene; organic dyes, such as methylene blue; some charge-transfer molecular complexes; and ion-radical salts. Fig. 1.1 shows the chemical structures of several representative families of COMs. Our research attention was paid to conductive polymers and oligomers.



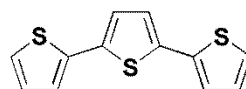
polyacetylene



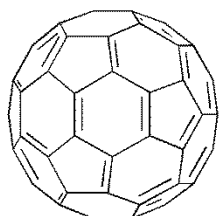
poly(3-alkylthiophene)



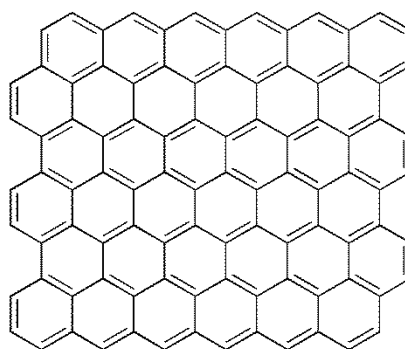
poly(p-phenylene vinylene)



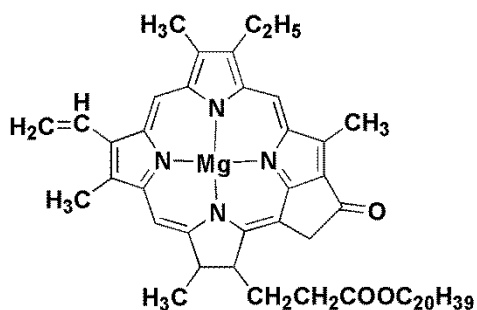
oligothiophene



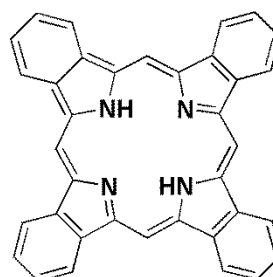
fullerene



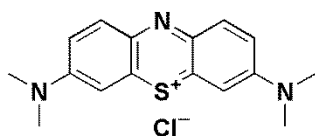
graphene



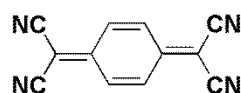
chlorophyll a



phthalocyanine



methylene blue



7,7,8,8-Tetracyanoquinodimethan

Fig. 1.1 Chemical structures of several representative families of COMs

1.1.2 Structures and properties

So far, a great progress has been accomplished in synthesis of COMs and in characterization of their structure and properties.^[10-12] The essential structural characteristics of COMs are the conjugate π -electron systems, which is formed by the p_z orbital of sp^2 -hybridized C atoms in the molecules (Fig. 1.2). CH=CH unit is the simplest constituent of this type of materials. When the constituent molecules of organics have π -conjugate systems, electrons can move via π -electron cloud overlaps, especially by hopping, tunnelling and related mechanisms.

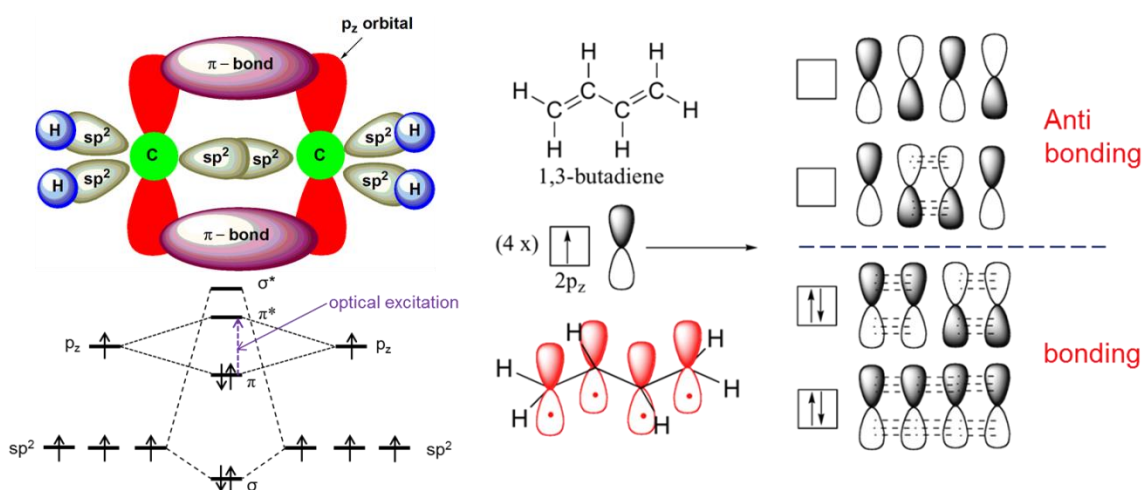


Fig. 1.2 Scheme of the orbitals and bonds for two and four sp^2 -hybridised carbon atoms

Significantly, π bonding is weak. Therefore, the lowest electronic excitations of conjugated molecules are the π - π^* transitions with an energy gap typically between 1.5 and 3eV leading to light absorption or emission in the visible spectral range. In detail, the electronic properties of a molecule depend on factors like the conjugation length or

the presence of electron donating or withdrawing groups.^[13,14] Thus organic chemistry offers a wide range of possibilities to tune the optoelectronic properties of COMs materials. Electronic excitations, called π - π^* transitions lead to two important properties for COMs:

(1) Optical properties

The absorption of light causes a molecular excitation that can migrate through the crystal in the form of excitons.^[15] The formation of charge carriers under the action of light is due to the decay of excitons on the surface of the crystal, at structural defects, and at impurities when exciton-exciton interaction occurs; it may also be due to the autoionization of highly excited molecules. On the other hand, as a consequence of this weak electronic delocalization, organic semiconductors have two important peculiarities. One is the existence of well-defined spin states (singlet and triplet) as in isolated molecules which has important consequences for the photophysics of these materials.^[16] Usually the ground state of an organic molecule is a singlet state (S0) and absorption of a photon leads to the first excited singlet state (S1). Thereby the Franck–Condon factor determines the relative intensities of the vibronic transitions within this manifold. Typical lifetimes of the S1 state are in the range 1–10ns, thus leading to a rapid transition back to the S0 ground state via fluorescence or nonradiative transitions.^[17,18] In the excited singlet state there is a small probability for intersystem crossing to the triplet state (T1), from which the excitation energy can be released either by phosphorescence or non-radiatively. However, since intersystem crossing is a weak process, triplet lifetimes are usually in the millisecond range for pure aromatic hydrocarbons, and radiative decay via phosphorescence is usually not observed at room temperature. A second important

difference originates from the fact that optical excitations (“excitons”) are usually localized on one molecule and therefore have a considerable binding energy. A simple estimation as the Coulomb energy of an electron-hole pair localized at a distance of 10 Å in a medium with a dielectric constant of 3 yields a value of about 0.5 eV for the exciton binding energy. In photovoltaic cells this binding energy has to be overcome before a pair of independent positive and negative charge carriers is generated.

(2) Charge transport

The activation energy necessary to form charge carriers in organic semiconductors decreases as the number of conjugations in the molecule increases, and in polymers it may be of the order of the thermal energy.^[19] Charge transport in organic semiconductors is dependent on π -bonding orbitals and quantum mechanical wave-function overlap. In disordered organic semiconductors, there is limited π -bonding overlapping between molecules and conduction of charge carriers (electrons or holes) is described by quantum mechanical tunnelling.^[20] Charge transport depends on the ability of the charge carriers to pass from one molecule to another. Because of the quantum mechanical tunnelling nature of the charge transport, and its subsequent dependence on a probability function, this transport process is commonly referred to as hopping transport.^[21] Hopping of charge carriers from molecule to molecule depends upon the energy gap between HOMO and LUMO levels. Carrier mobility is reliant upon the abundance of similar energy levels for the electrons or holes to move to and hence will experience regions of faster and slower hopping. This can be affected by both the temperature and the electric field across the system. A theoretical study^[22] has shown that in a

low electric field the conductivity of organic semiconductor is proportional to $T^{-1/4}$ and in a high electric field is proportional to $e^{-(E/aT)}$, where a is a constant of the material. Another study shows that the conductivity of the organic semiconductor pentacene is frequency-dependent and provided evidence that this behavior is due to its polycrystalline structure and hopping conduction.^[23]

It has been shown that intrinsic charge carrier transport in some sufficiently pure and perfect low molecular weight organic crystals can safely be described within the framework of coherent Bloch-type band states as long as temperature is sufficiently low. Low temperature mobilities can reach values as high as $105 \text{ cm}^2/(\text{V s})$, with effective masses close to the free electron mass.^[24-27] Upon increasing temperature, increased phonon scattering slows down band transport, whence the local polarization interactions increase and, hence, the effective mass grows, in conjunction with band narrowing. The charge carriers get increasingly dressed with a polarization cloud leading to successively slower polaron-band conduction. Finally a second, parallel transport channel, thermally activated polaron-hopping transport, is more efficient and takes over. It has recently been shown for a number of materials that this transition is a rather general feature.^[28] For crystallographic directions with especially weak p-electronic interactions as well as for crystal structures with specific intermolecular interactions (molecular sandwich pairs), electronic transport, however, can be governed by polaron-hopping in a wide temperature range. Orientational molecular disorder in an otherwise perfect crystal lattice fully suppresses band transport.

1.1.3 Applications, processing and characterization

Applications: COMs have a very promising future, and they permit the fabrication of solar modules with several potential advantages, including light weight, flexibility, low cost synthesis and production, the possibility of creating large-area devices, and easy manufacture of thin film devices by vacuum evaporation/sublimation or solution cast or printing technologies.^[29-39] Furthermore, organic semiconductor thin films may show high absorption coefficients.^[40,41] Various of excellent advantages and properties leading to the general optoelectronic applications.^[42-44] We list our interest as follow:

- ① An important device application of organic semiconductors is in organic photovoltaic cells (OPVCs). In spite of their high absorption coefficient, which exceeds 10^5 cm^{-1} in most materials, the application of organic semiconductors in OPVCs faces the problem of the large exciton binding energy which prohibits efficient exciton dissociation. This can be overcome by making use of a photoinduced charge transfer between an electron donor like PPV and the fullerene C_{60} as an acceptor.^[45] Due to the short exciton diffusion length of typically 10nm, efficient OPVCs use the so-called bulk-heterojunction concept of mixing donor and acceptor in one single layer. In spite of the huge progress recently achieved, there are still challenges to achieve sufficient lifetime of OPVCs under ambient conditions or the availability of low-band gap materials to make better use of the solar spectrum.^[46]

- ② The field-effect transistor (FET) is a transistor that uses an electric field to control the shape and hence the conductivity of a channel of one type of charge carrier in a semiconductor material.^[47] FETs are unipolar transistors as they

involve single-carrier-type operation. The concept of the FET predates the bipolar junction transistor (BJT), though it was not physically implemented until after BJTs due to the limitations of semiconductor materials and the relative ease of manufacturing BJTs compared to FETs at the time. Organic FETs are 3-terminal devices in which the charge carrier density in the channel between source and drain contacts can be controlled by the applied gate voltage across a thin dielectric.^[48,49] The drain current is then given by

$$I_D = \frac{W}{L} C_i \mu (V_G - V_T) V_D$$

in the linear region, and by

$$I_D = \frac{W}{2L} C_i \mu (V_G - V_T)^2$$

in the saturation regime. Here W/L denotes the ratio between channel width and length, C_i the specific insulator capacitance and V_T the threshold voltage. Thus the performance of OFETs can be tuned to some degree by using suitable geometries with short channel length L or thin insulating layers of materials with high dielectric constant, but it is clear that the mobility μ also needs to be high (in the range of amorphous Si) to enable switching at frequencies significantly higher than 100 kHz which will be needed for more demanding applications in the future. This requires materials and methods to grow highly ordered organic semiconductor films. A further challenge will be to realize CMOS-like organic integrated circuits by using materials with stable p- and n-conducting properties.

Processing: There are significant differences between the processing of small molecule organic semiconductors and semiconducting polymers. Thin films of soluble conjugated polymers can be prepared by solution processing methods. On the other hand, small molecules are quite often insoluble and typically require deposition via vacuum sublimation. Both of approaches yield amorphous or polycrystalline films with variable degree of disorder. “Wet” coating techniques require polymers to be dissolved in a volatile solvent, filtered and deposited onto a substrate. Common examples of solvent-based coating techniques include drop casting, spin-coating, doctor-blading, inkjet printing and screen printing.^[50] Spin-coating is a widely used technique for small area thin film production. It may result in a high material loss. The doctor-blade technique has a minimal material loss and was primarily developed for large area thin film production. Vacuum based thermal deposition of small molecules requires evaporation of molecules from a hot source. The molecules are then transported through vacuum onto a substrate. Condensation of these molecules on the substrate surface results in thin film formation. Wet coating techniques can be applied to small molecules but to a lesser extent depending on material solubility.

Characterization: In order to design and model the organic semiconductors, such optical properties as absorption and photoluminescence need to be characterized.^[51,52] Optical characterization for this class of materials can be done using UV-visible absorption spectrophotometers and photoluminescence spectrometers. Semiconductor film appearance and morphology can be studied with atomic force microscopy (AFM) and scanning electron microscopy (SEM). Electronic properties such as ionisation

potential can be characterized by probing the electronic band structure with ultraviolet photoelectron spectroscopy (UPS).^[53] The charge-carrier transport properties of organic semiconductors are examined by a number of techniques. For example, time-of-flight (TOF) and space charge limited current techniques are used to characterize “bulk” conduction properties of organic films. Organic field effect transistor (OFET) characterization technique is probing “interfacial” properties of semiconductor films and allows to study the charge carrier mobility, transistor threshold voltage and other FET parameters. OFETs development can directly lead to novel device applications such as organic-based flexible circuits, printable radio frequency identification tags (RFID) and active matrix backplanes for displays.^[54,55] Chemical composition and structure of organic semiconductors can be characterized by infrared spectroscopy, secondary ion mass spectrometry (SIMS) and X-ray photoelectron spectroscopy (XPS).

1.2 Principle of polymer solar cells with bulk heterojunction structure

Bulk heterojunction polymer solar cell is a representative type of photovoltaics based on COMs. In this type of photovoltaic cell, the electron donor and acceptor are mixed together, forming a polymer blend (Figure 1.3). If the length scale of the blend is similar to the exciton diffusion length, most of the excitons generated in either material may reach the interface, where excitons break efficiently. Electrons move to the acceptor domains then were carried through the device and collected by one electrode, and holes were pulled in the opposite direction and collected at the other side.^[56-58]

The flow of the progress can be diagramed as follow (Fig. 1.3):^[59]

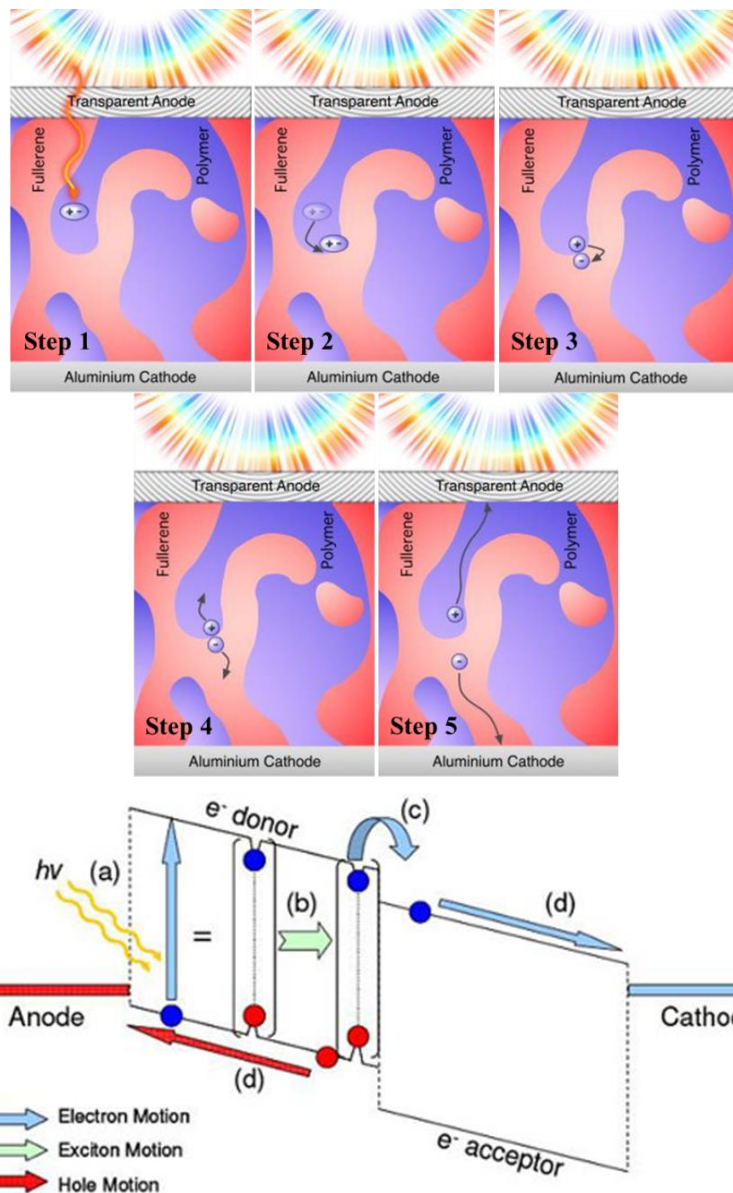


Fig. 1.3 Diagram of how the solar cells work

Step 1: Light Absorption => Exciton Generation

Light is absorbed in the donor material, e.g., a conjugated polymer, excitons are thus created.

Step 2: Exciton Diffusion => to Acceptor Interface

The photogenerated excitons are strongly Coulomb bound due to the low dielectric

constant in organic materials, and electrically neutral excitons can only move by diffusion with the diffusion length of only a few nanometres. In order to dissociate into an electron-hole pair, it has to find an acceptor site (e.g., fullerene molecule). The photovoltaic cells with bulk heterojunction of intermixed donor and acceptor materials (shown in the figure), such as conjugated polymers blended with fullerene derivatives, leads to the interface much enough for dissociation.

Step 3: Exciton Dissociation => Polaron Pair Generation

Excitons dissociate only at energetically favourable acceptor molecules such as the fullerenes. When the energy gain is larger than the exciton binding energy, an electron transfer (or charge transfer) takes place, that is the exciton was dissociated into an electron on the fullerene acceptor, and a hole remaining on the polymer. This electron-hole pair is still Coulomb bound, and is called geminate pair or polaron pair

Step 4: Polaron Pair Dissociation => Free Electron-Hole Pairs

The polaron pairs are Coulomb bound and also need to be dissociated, this time by an electric field (= built-in voltage + applied voltage).

Step 5: Charge Transport => Photocurrent

The electrons and holes are transported to the respective electrodes, driven by the electric field, and moved by a hopping transport process. A loss of free charge carriers was caused by nongeminate recombination during the charge transport to the contacts.

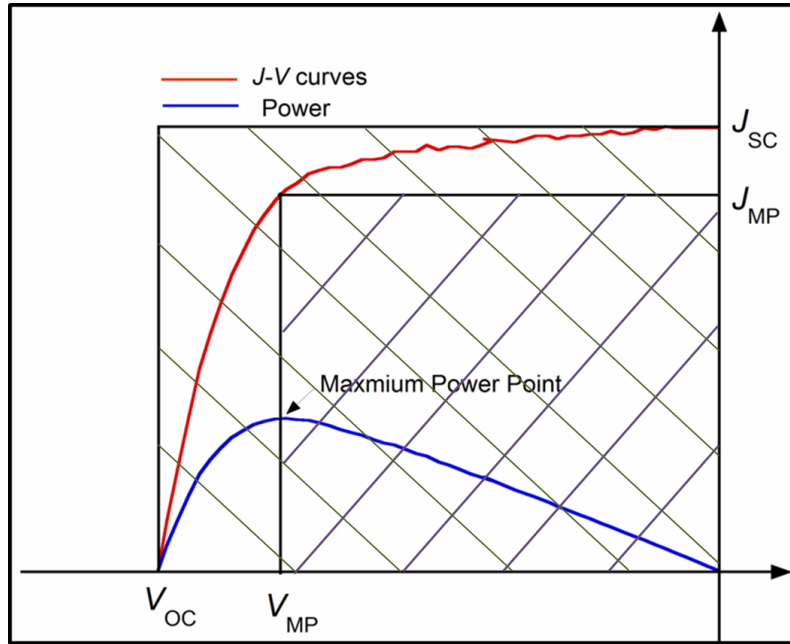


Fig. 1.4 Current-voltage curves of the organic solar cells.

The current-voltage characteristics of a solar cell in the dark and under illumination are shown in Fig. 1.4. In the fourth quadrant (between (V_{oc}) and (J_{sc})), the device generates power under light. At Maximum Power Point (MPP), the product of current and voltage is the largest.^[60]

The photovoltaic power conversion efficiency of a solar cell is determined by the following formula:

$$\eta = \frac{V_{OC} * J_{SC} * FF}{P_{in}}$$

$$FF = \frac{V_{MP} * J_{MP}}{V_{OC} * J_{SC}}$$

where V_{oc} is the open circuit voltage, J_{sc} is the short circuit current, FF is the fill factor,

and P_{in} is the incident light power density. This light intensity is standardized at 1000 W/m² with a spectral intensity distribution matching that of the sun on the earth's surface at an incident angle of 48.2°, which is called the AM 1.5 spectrum.^[61] J_{MP} and V_{MP} are the current and voltage at the maximum power point.

1.6.1. Parameters for Solar Cell Efficiency

Open Circuit Voltage (V_{oc}). Generally, the open circuit voltage of a metal-insulator-metal (MIM) device is determined by the difference in work functions of the two metal contacts.^[62] However, in a p-n junction, the maximum available voltage is determined by the difference of the quasi Fermi levels of the two charge carriers, that is, n-doped semiconductor energy level and p-doped semiconductor energy level, respectively. In organic solar cells, the open circuit voltage is found to be linearly dependent on the highest occupied molecular orbital HOMO level of the donor (p-type semiconductor quasi Fermi level) and lowest unoccupied molecular orbital LUMO level of the acceptor (n-type semiconductor quasi Fermi level).^[63,64]

Short Circuit Current. (J_{sc}) The J_{sc} is determined by the amount of absorbed light and the internal conversion efficiency. An experimentally accessible value is the external quantum efficiency or incident photon to current efficiency, IPCE [%], defined and calculated using follow equation.

$$IPCE = \frac{1240 * J_{sc}}{\lambda * P_{in}}$$

where λ [nm] is the incident photon wavelength, J_{SC} [mA cm⁻²] is the photocurrent of the device and P_{in} [W m⁻²] is the incident power. The internal quantum efficiency, the ratio of external current to absorbed photons, is estimated to be close to 100% for conjugated polymer-fullerene blends. For an increase in the photocurrent, the light absorption has to be increased. Increasing the thickness is limited due to the low mobility of the charges and possible recombination losses.^[65]

Fill Factor. Fill factor is determined by charge carriers reaching the electrodes, when the built-in field is lowered toward the open circuit voltage. In fact, there is a competition between charge carrier recombination and transport. The nanomorphology of donor/acceptor composites is known to have an important influence on device efficiency.^[66] Furthermore, the series resistances influence the filling factor considerably and should be minimized. Finite conductivity of the ITO substrate clearly limits the *FF* on large area solar cells.^[67] Finally, the device should be free of “shorts” between electrodes to maximize the parallel shunt resistance.

1.3 The aim of the present work

As mentioned above, our research attention was paid to the conductive polymers and oligomers. In this thesis, the author describes the synthesis of novel π -conjugated oligomers and D-A type copolymers for optoelectronic applications.

In chapter 2, Novel copolymers (**PM1** and **PM2**) comprising (E)-2,3-bis(2-thienyl)acrylonitrile and benzo[1,2-b;4,5-b']dithiophene derivatives are designed and synthesized to be applied as an electron donor material in polymer solar

cells blended with PC₆₁BM as an electron acceptor. These copolymers show a good thermal stability with a 5% weight loss temperature beyond 340 °C, and their films exhibit a broad absorption band with a low optical bandgap of ca. 1.84 eV. Polymer solar cells based on **PM2**, prepared under optimized preparation conditions, are found to exhibit a short-circuit photocurrent of 10.71 mA/cm², an open-circuit photovoltage of 600 mV, a fill factor of 65%, and a power conversion efficiency of 4.17% under AM 1.5 illumination conditions, 100 mW/cm².

In chapter 3, poly[(benzodithiophene-2,6-diyl)(2,5-thienylene)] (**PS0**) and its derivatives with π -conjugated side-chains (**PS1**: thienylethenyl and **PS2**: thienylcyanoethenyl) were designed and synthesized in order to study the effects of the conjugated side-chains on the optical, electrochemical, and photovoltaic properties of the copolymers. It was found that the electronic properties and energy levels of the copolymers can be effectively tuned through changing a conjugated side-chain attached to a polymer backbone. Polymer solar cells based on copolymer/PC₆₁BM exhibited power conversion efficiencies of 2.85%, 3.44%, and 4.49%, respectively, for **PS0**, **PS1**, and **PS2** under a simulated solar light (AM1.5G, 100 mW/cm²), compared with 4.17% for a main-chain type copolymer corresponding to **PM2**. The results reveal that the introduction of the conjugated side-chain with an electron-deficient group to a polymer backbone is an effective approach for improving the performance of the photovoltaic materials.

In chapter 4, Five sorts of soluble oligothiophenes (trimer to undecamer) containing 3,4-ethylenedioxythiophene (EDOT) were synthesized, and their optical and electrochemical properties were investigated in relation to the chain length of oligothiophenes and the number of EDOT units. The introduction of the EDOT unit into

a main oligothiénylene unit induced a red shift of absorption bands and a negative shift of oxidation potentials. The conductivity of an electrochemically oxidized film of undecamer was found to be around 1 S/cm. A thin-film field effect transistor was preliminary fabricated with neutral undecamer films and the hole mobility was determined.

1.4 References

1. H. Letheby, *J. Chem. Soc.*, 1862, **15**, 161.
2. Wikipedia [EB/OL]. http://en.wikipedia.org/wiki/Organic_semiconductor.
3. H. Naarmann. “*Polymers, Electrically Conducting*” in Ullmann’s Encyclopedia of Industrial Chemistry, Wiley-VCH, Weinheim, 2002.
4. M. Jozefowicz, L. T. Yu, G. Berlorgey, and R. Buvet, *J. Polym. Sci. Part C*, 1967, **16**, 2943.
5. A. Dall’Ollio, Y. Dascola, G. P. Gardini, and C. R., *Acad.Sci.*, 1969, **267**,4336.
6. C. K. Chiang, C. R. Fincher, Y. W. Park, A. J. Heeger, H. Shirakawa, E. J. Louis, and A. G. MacDiarmid, *Phys. Rev. Lett.*, 1977, **39**, 1098.
7. H. Shirakawa, E. J. Louis, A. G. MacDiarmid, C. K. Chiang, and A. J. Heeger. *J. Chem. Soc., Chem. Commun.*, 1977, **16**. 578-580.
8. The noble prize in chemistry, 2000: conductive polymers, nobleprize.org.
9. R. Farchioni, G. Grosso, *Organic Electronic Materials*. Springer, Berlin, 2001.
10. G. R. Hutchison, Y.J. Zhao, B. Delley, A. J. Freeman, M. A. Ratner, and T. J. Marks, *Phys. Rev. B*, 2003, **68**, 035204.
11. J. W. vanderHorst, P. A. Bobbert, M. A. J. Michels, G. Brocks, and P. J. Kelly, *Phys. Rev. Lett.*, 1999, **83**, 4413.
12. K. Yoshino, Y. Kohno, T. Shiraishi, K. Kaneto, S. Inoue, and K. Tsukagoshi, *Synth. Met.*, 1985, **10**, 319.
13. Y. Luo, P. Norman, K. Ruud, and H. Agren, *Chem. Phys. Lett.*, 1998 **285**, 160.

14. J. S. de Melo, L. M. Silva, L. G. Arnaut, and R. S. Becker, *J.Chem. Phys.*, 1999 **111**, 5427.
15. W. Brütting, in “*Organic Semiconductors*”, 2005
16. J. Poncali. *Chem. Rev.*, 1992, **92**. 711.
17. T. C. Chung, J. H. Kaufman, A. J. Heeger, and F. Wudl, *Phys.Rev.B*, 1984, **30**, 702.
18. G. Tourillon, D. Gourier, F. Garnier, and D. Vivien, *J. Phys. Chem.*, 1984, **88**, 1049.
19. H. Bassler, and A. Kohler, *Top. Curr. Chem.*, 2012, **312**, 1.
20. N. Alexei, *Organic And Inorganic Nanostructures*, Artech House Publishers, 2005.
21. J. Hirsch, *J. Phys. C: Solid State Phys.*, 1979, **12**, 321.
22. L. Li, G. Meller, and H. Kosina, *Microelectronics J.*, 2007, **38**, 47.
23. D. R. Lenski, A. Southard, and M. S. Fuhrer. *Appl. Phys. Lett.*, 2009, **94**, 232103.
24. W. Warta, and N. Karl, *Phys. Rev. B*, 1985, **32** 1172.
25. N. Karl, J. Marktanner, R. Stehle, and W. Warta, *Synth. Met.*, 1991 **42-43**, 2473.
26. J.H. Schon, C. Kloc, and B. Batlogg, *Phys. Rev. Lett.*, 2001, **86**, 3843.
27. J.H. Schon, C. Kloc, and B. Batlogg, *Science*, 2000, **288**, 2338.
28. N. Karl, *Synth. Met.*, 2003, **133-134**, 649–657
29. S. E. Shaheen, D. S. Ginley, and G. E. Jabbour, *MRS Bull.*, 2005, **30**, 10.
30. P. Peumans,; A. Yakimov, and S. R. Forrest, *J. Appl. Phys.*, 2003, **93**, 3693.
31. S. S. Sun, and N. S. Sariciftci, *Organic Photovoltaics: Mechanisms, Materials, and Devices*; Taylor and Francis: Boca Raton, FL, 2005.
32. S. Gunes, H. Neugebauer, and N. S. Sariciftci, *Chem. Rev.*, 2007, **107**, 1324.
33. M. D McGehee, *MRS Bull.*, 2009, **34**, 95.

34. Shaheen, S. E.; Ginley, and D. S. Dekker, *Encyclopedia of Nanoscience and Nanotechnology*, New York, 2004.
35. D. Placencia, W. Wang, R. C. Shallcross, K. W. Nebesny, M. Brumbach, and N. R. Armstrong, *Adv. Funct. Mater.*, 2009, **19**, 1913.
36. F. Yang, M. Shtein, and S. R Forrest, *Nat. Mater.*, 2005, **4**, 37.
37. S. Yoo, B. Domercq, and B. Kippelen, *Appl. Phys. Lett.*, 2004, **85**, 5427.
38. A. Kulkarni, C. Tonzola, A. Babel, and S. Jenekhe, *Chem. Mater.*, 2004, **16**, 4556.
39. K. Y. Law, *Chem. Rev.*, 1993, **93**, 449.
40. J. M. Giaimo, J. V. Lockard, L. E. Sinks, A. M. Scott, T. M. Wilson, and M. R. Wasielewski, *J. Phys. Chem. A*, 2008, **112**, 2322.
41. H. Ohkita, S. Cook, Y. Astuti, W. Duffy, S. Tierney, W. Zhang, M. Heeney, I. McCulloch, J. Nelson, D. D. C. Bradley, and J. R. Durrant, *J. Am. Chem. Soc.*, 2008, **130**, 3030.
42. A. W. Hains, Z. Liang, M. A. Woodhouse, and B. A. Gregg, *Chem. Rev.*, 2010, **110**, 6689.
43. V. Coropceanu, J. Cornil, D. A. Filho, Y. Olivier, R. Silbey, and J. L. Bredas, *Chem. Rev.*, 2007, **107**, 926.
44. K. Walzer, B. Maennig, M. Pfeiffer, and K. Leo, *Chem. Rev.*, 2007, **107**, 1233.
45. N. S. Sariciftci, L. Smilowitz, A. J. Heeger, and F. Wudl, *Science*, 1992, **258**, 1474.
46. C. J. Brabec, V. Dyakonov, J. Parisi, and N. S. Sariciftci, *Organic Photovoltaics*. Springer, Berlin, 2003.
47. Wikipedia [EB/OL]. http://en.wikipedia.org/wiki/Field-effect_transistor.
48. G. Horowitz, *Adv. Mater.*, 1998, **10**, 365.
49. C. Dimitrakopoulos, and P. R. L. Malenfant, *Adv. Mater.*, 2002, **14**, 99.

50. F. Faupel, C. Dimitrakopoulos, A. Kahn, and C. Woll, *J. Mater. Res.*, 2004, **19**, 7.
51. B. Masenelli, S. Callard, A. Gagnaire, and J. Joseph, *Thin Solid Films*, 2000 **364**, 264.
52. L. G. Wang, H. W. Zhang, X. L. Tang, Y. Q. Song, Z. Y. Zhong, and Y. X. Li, *Phys. Scr.*, 2011, **84**, 045701.
53. W. R. Salaneck, and A. Kahn. *Conjugated polymer and molecular interfaces*. CRC Press, 2002.
54. W. Brütting, *Physics of organic semiconductors*. Wiley-VCH. (2005).
55. D. René, D. Arindam, and Grell. Martin, *J. Phys. D: Appl. Phys.*, 2007, **40**, 3563.
56. H. Hoppe, and N. S. Sariciftci, *J. Mater. Chem.*, 2004, **19**, 1924.
57. J. Nelson. *Curr. Opin. Solid State Mater. Sci.*, 2002, **6**, 87.
58. D. Kearns, M. Calvin, *J. Chem. Phys.*, 1958, **29**, 950.
59. Deibel, C. [EB/OL]. <http://blog.disorderedmatter.eu/page/11/>.
60. S. Gunes, H. Neugebauer, and N. S. Sariciftci. *Chem. Rev.*, 2007, **107**, 1324.
61. J. Rostalski, and D. Meissner, *Sol. Energy Mater. Sol. Cells.*, 2000, **61**, 87.
62. I. Parker, *J. Appl. Phys.*, 1994, **75**, 1656.
63. C. J. Brabec, A. Cravino, D. Meissner, N. S. Sariciftci, T. Fromherz, M. Minse, L. Sanchez, and J. C. Hummelen, *Adv. Funct. Mater.*, 2001, **11**, 374.
64. M. Scharber, D. Muhlbacher, M. Koppe, P. Denk, C. Waldauf, A. J. Heeger, and C. Brabec, *Adv. Mater.*, 2006, **18**, 789.
65. C. Winder, and N. S. Sariciftci, *J. Mater. Chem.*, 2004, **14**, 1077.
66. P. Peumans, S. Uchida, and S. Forrest, *Nature*, 2003, **425**, 158.
67. I. Riedel, and V. Dyakonov, *Phys. Status Solidi A*, 2004, **201**, 1332.

Chapter 2

Synthesis and Photovoltaic Applications of Main-chain Type Polymers with Benzodithiophene and Bisthienylacrylonitrile Units

2.1 Introduction

Development of clean energy sources capable of replacing environment-polluting fossil fuels is a very urgent subject for every energy researcher.^[1,2] Undoubtedly, solar energy is one of the most environment-friendly, sustainable, and promising resources and various types of photovoltaic devices have been developed for conversion of solar energy to electricity. Among them, bulk heterojunction (BHJ) solar cells or polymer solar cells (PSCs), which consist of a donor-type conjugated polymer and an acceptor-type fullerene derivative, have received a strong interest because of low-cost, lightweight and easy fabrication.^[3-6] There are many requirements for the polymer applied in PSC. Energy levels of a polymer to be used as a donor material in PSCs should be tuned so as to have a low-lying highest occupied molecular orbital (HOMO) level to provide a large open-circuit photovoltage (V_{oc}) and a suitable lowest unoccupied molecular orbital (LUMO) level to provide enough offset for light-induced charge separation.^[7] In addition to the suitable energy level matching with the fullerene acceptor, the donor polymer should exhibit broad absorptions with high absorption coefficients toward sunlight, high hole mobility, and appropriate compatibility with the

fullerene to form nanoscale bicontinuous interpenetrating network.^[8-11] One plausible approach toward this goal is to design alternate copolymers comprising electron-rich (D) and electron-deficient (A) units with some specific functional groups.^[12-14] Until now, many candidates for D and A units have been reported. Among them, we have focused our attention on (*E*)-2,3-bis-(2-thienyl)acrylonitrile (BTA) as an A unit since BTA possesses a strong electron-accepting cyano group with a thienylene-vinylene moiety which has an extended π -conjugation length responsible for the efficient light harvesting.^[15-19] A few D-A type copolymers incorporating a BTA unit have been reported.^[20-26] To date, however, PSCs based on the BTA-containing copolymers have failed to yield high power conversion efficiencies (PCEs). To enhance the PCEs of solar cells, other types of D units to be combined with BTA should be developed.

Recently, much attention has been given to benzo[1,2-*b*;4,5-*b'*]dithiophene (BDT) as a D unit. The absorption spectrum of BDT-containing copolymers covers the whole visible region from 350 to 750 nm, and the solar cells based on BDT copolymers have yielded high PCEs of 3-6%.^[27-29] It is also known that side alkoxy groups attached to the BDT unit play a significant role for enhancing photovoltaic properties by making a bandgap of the polymer narrower and facilitating an electron transfer from the donor polymer to fullerene.

In the present study, we designed two new copolymers consisting of BTA as an electron-deficient group and BDT as an electron-rich group: poly[(4,8-dihexyloxybenzo[1,2-*b*;4,5-*b'*]dithiophene)-*alt*-((*E*)-2,3-bis(2-thienyl)acrylonitrile)] (**PM1**) and poly[(4,8-didecyloxybenzo[1,2-*b*;4,5-*b'*]dithiophene)-*alt*-((*E*)-2,3-bis(2-thienyl)acrylonitrile)] (**PM2**). The combination of BTA and BDT units is expected to give rise to superior photovoltaic performances by utilizing distinguished

characteristics of both BTA and BDT. The synthesis and characterizations of the copolymers are described, together with the performances of PSCs prepared under different conditions with the two polymers blended with PC₆₁BM as the active layer.

2.2 Experimental

2.2.1 Materials

Thiophene-3-carbonyl chloride, diethylamine, hexyl-*p*-toluenesulfonate, 1-bromodecane, *n*-butyllithium (*n*-BuLi, 1.67 M solution in hexane), trimethyltinchloride (1.0 M solution in hexane), 2-thiophenecarboxaldehyde, tetrakis(triphenylphosphine)palladium(0) (Pd(PPh₃)₄), 2-(2-thienyl)acetonitrile, sodium methoxide and poly(3,4-ethylenedioxythiophene):poly(styrenesulfonate) (PEDOT:PSS, Baytron PH500) were purchased from Tokyo Chemical Industry and used without purification. Tetrabutylammonium bromide (TBAB), *N*-bromosuccinimide (NBS), and tetrabutylammonium hexafluorophosphate (TBAPF₆) were purified by recrystallization. Tetrahydrofuran (THF), toluene, and acetonitrile (CH₃CN) were refluxed over CaH₂, Na, and P₂O₅, respectively, and then distilled under nitrogen prior to use. *N,N*-Dimethylformamide (DMF) was distilled prior to use. Column chromatography was employed on silica gel 60N (spherical neutral).

2.2.2 Measurement and Characterization

The NMR was recorded using a Varian 500 MHz instrument and chemical shifts

were recorded in parts per million. The ultraviolet-visible (UV-vis) absorption spectrum was recorded on a Shimadzu UV-3150 spectrophotometer and FT-IR spectra were obtained with a PerkinElmer FT-IR spectrometer. Polymer molecular weights and polydispersity index (PDI) were measured by gel permeation chromatography (GPC) analysis using Shimadzu chromatograph with Shodex KF801, KF802, and KF803L columns at 40 °C with THF as eluent. Thermogravimetric analysis (TGA) was conducted with a SIC model TG/DTA-6200 at a heating rate of 10 °C min⁻¹ under nitrogen flow. Electrochemical measurements were performed at room temperature (RT) using a Hokuto Denko HSV-100 automatic polarization system under an argon atmosphere. A three-electrode cell equipped with a platinum sphere working electrode, an Ag/Ag⁺ (0.01 M in CH₃CN) reference electrode, and a platinum wire counter electrode was applied. All samples were measured in CH₃CN solutions containing 0.1 M TBAPF₆ as a supporting electrolyte. Ferrocene/ferrocenium redox couple (Fc/Fc⁺) was used as an internal reference.

2.2.3 Device fabrication and photovoltaic evaluations

Devices with a typical sandwich structure of ITO/PEDOT:PSS/polymer:PC₆₁BM/LiF/Al were fabricated (Fig. 1). Indium-tin oxide (ITO)-coated glass substrates were etched by mixed acidic solution (HCl:HNO₃:H₂O=4:3:6) and cleaned stepwise under ultrasonication in detergent, alkali solution, de-ionized water, acetone, and 2-propanol for 10 min, respectively, then treated with UV ozone for 30 min. PEDOT:PSS was spin-coated from an aqueous solution on top ITO substrate as buffer layer giving a thickness of about 30 nm, then it was heated on a

hot plate at 100 °C for 10 min. Subsequently, a blend solution of polymer/PC₆₁BM (1:1 w/w) with concentration of 15 mg mL⁻¹ in chlorobenzene with or without 1,8-diiodooctane (DIO, 3 vol%) was spin-coated after being filtrated through a 0.20 μm syringe filter (PTFE) on top of PEDOT:PSS film giving a thickness of about 100 nm, and annealing of the blend film was performed at 150 °C for 10 min. The devices were completed by depositing LiF (0.6 nm) and Al (100 nm) cathode as top electrodes with area defined by a shadow mask under high vacuum (< 2 x10⁻⁶ Torr) and annealed at 150 °C, producing an active area of 25 mm² for each cell. Photocurrent-voltage characteristics were measured under filtered light illumination from an Asahi HAL-302 solar simulator (AM 1.5 G, 100 mW cm⁻²) in an ambient environment. Data were recorded with a computer-controlled Hokuto Denko sourcemeter.

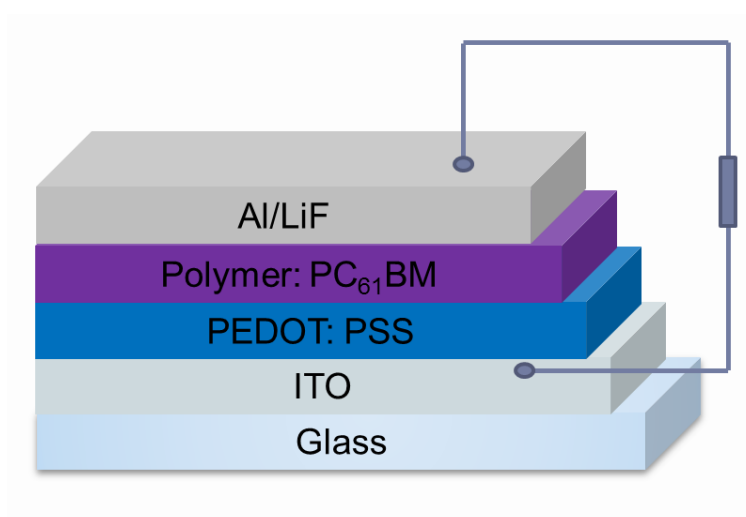
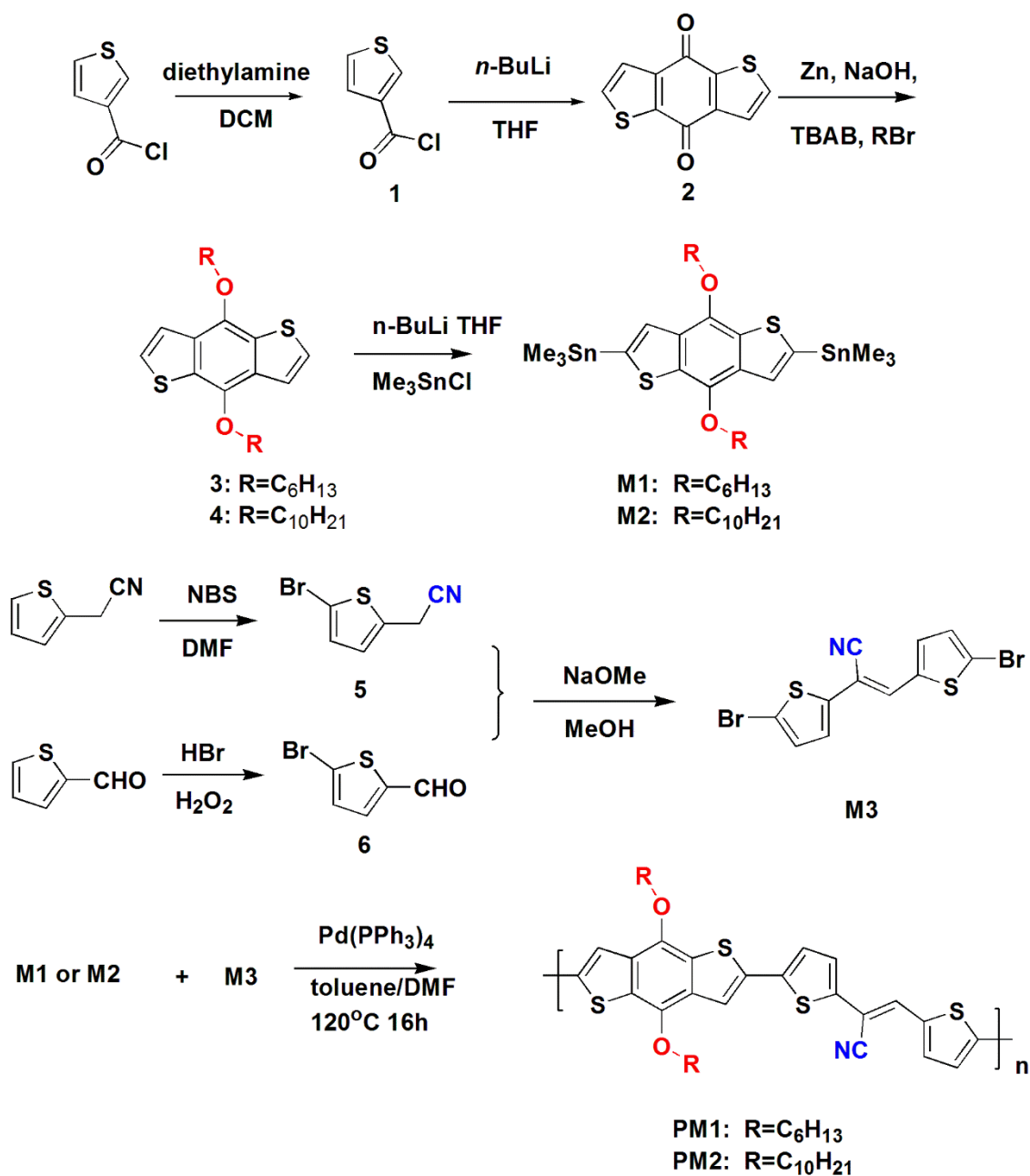


Fig. 2.1 Schematic device architecture for polymer/fullerene solar cells. The active layer is sandwiched between two electrodes: the ITO electrode covered with PEDOT:PSS layer and the LiF/Al top electrode.

2.2.4 Synthetic procedures

The synthetic routes of the monomers and copolymers are shown in Scheme 1. The detailed synthetic procedures are as follows:



Scheme 2.1 Synthesis routes of the monomers and corresponding copolymers.

N,N-Diethylthiophene-3-carboxamide (1)

In a 50 mL flask in ice-water bath, diethylamine (6.25 mL, 4.38 g, 60 mmol) and CH₂Cl₂ (10 mL) were mixed, and the solution of thiophene-3-carbonyl chloride (4.25 g, 30 mmol in 10 mL of CH₂Cl₂) was added into the flask slowly.^[27] After all of the solution was added, the ice-water bath was removed, and the reactant was stirred at RT for 30 min. Then, the reactant was washed by water several times and the organic layer was dried over anhydrous MgSO₄. After removing solvent, the crude product was purified by distillation under vacuum and compound **2** was obtained as pale yellow oil (4.9 g, 27 mmol). Yield: 90.0%. ¹H NMR (500 MHz, CDCl₃, ppm): δ 7.48 (s, 1H), 7.32 (d, *J* = 5 Hz, 1H), 7.20 (d, *J* = 5 Hz, 1H), 3.40 (m, 4H), 1.20 (t, *J* = 6 Hz, 6H). ¹³C NMR (500 MHz, CDCl₃, ppm): δ 165.0, 142.2, 137.4, 127.6, 124.5.

4,8-Dihydrobenzo[1,2-b:4,5-b']dithiophen-4,8-dione (2)

Compound **1** (20 mmol, 3.66 g) was put into a well-dried flask with THF (20 mL) under an inert atmosphere.^[27] The solution was cooled down by an ice-water bath, and *n*-BuLi solution (12 mL, 20 mmol, 1.67 M in hexane) was added into the flask dropwise within 30 min. Then, the reactant was stirred at RT for 1h. The reactant was poured into 50 g of ice water and stirred for 3 h. The mixture was filtrated, and the yellow precipitate was washed twice by water (20 mL), methanol (5 mL), and hexane (5 mL) successively. Compound **2** was obtained as a yellow powder (1.64 g, 7.45 mmol). Yield: 74.5%. ¹H NMR (500 MHz, CDCl₃, ppm): δ 7.70 (d, *J* = 5 Hz, 2 H), 7.66 (d, *J* = 5 Hz, 2 H). ¹³C NMR (500 MHz, CDCl₃, ppm): δ 174.5, 144.9, 142.8, 133.6, 126.6.

4,8-Dihexyloxybenzo[1,2-b:3,4-b']dithiophene (3)

Compound **2** (440 mg, 2 mmol), zinc powder (300 mg, 4.4 mmol), and water (15 mL) were put into a 100 mL flask; then sodium hydroxide (1.2 g) was added into the mixture. The mixture was well stirred and heated to reflux for 1 h. The color of the mixture changed from yellow to red during the reaction. Then, hexyl-*p*-toluenesulfonate (1.5 mL 4.4 mmol) and TBAB (140 mg, 0.44 mmol) were added into the flask. After being refluxed for 2 h, the reactant changed its color to orange. The reactant was poured into cold water and extracted by 100 mL of diethyl ether twice. The ether layer was dried over anhydrous MgSO₄. After removing solvent, the crude product was purified by recrystallization from ethanol. Compound **3** was obtained as a colorless crystal (460 mg, 1.18 mmol). Yield: 59.0%. ¹H NMR (500 MHz, CDCl₃, ppm): δ 7.51 (d, *J* = 5 Hz, 2H), 7.39 (d, *J* = 5 Hz, 2H), 4.28 (t, *J* = 6 Hz, 4H), 1.88 (m, 4H), 1.58 (m, 4H), 1.39 (m, 4H), 1.26 (m, 4H), 0.93 (t, *J* = 7 Hz, 6H). ¹³C NMR (500 MHz, CDCl₃, ppm): δ 131.6, 126.4, 121.5, 72.3, 32.5, 23.1, 14.0.

4,8-Didecyloxybenzo[1,2-*b*;3,4-*b'*]dithiophene (4)

The same procedure as for compound **3** was used. Compounds used were compound **2** (440 mg, 2 mmol), zinc powder (300 mg, 4.4 mmol), sodium hydroxide (1.2 g), 1-bromodecane (4.4 mmol) and a catalytic amount of TBAB (140 mg, 0.44 mmol), respectively. Compound **4** was obtained as a colorless crystal (553 mg, 1.1 mmol). Yield: 55.2%. ¹H NMR (500 MHz, CDCl₃, ppm): δ 7.48 (d, *J* = 5 Hz, 2H), 7.38 (d, *J* = 5 Hz, 2H), 4.29 (t, *J* = 6 Hz, 4H), 1.89 (m, 4H), 1.58 (m, 4H), 1.38-1.29 (m, 24H), 0.89 (t, *J* = 7 Hz, 6H). ¹³C NMR (500 MHz, CDCl₃, ppm): δ 131.5, 126.0, 120.3, 73.9, 31.9, 30.6, 29.6, 29.3, 26.1, 22.7, 14.1.

2,6-Bis(trimethylstannyl)-4,8-dihexyloxybenzo[1,2-b:4,5-b']dithiophene (M1)

Compound **3** (196 mg, 0.5 mmol) was dissolved in anhydrous THF (20 mL) and cooled in an acetone/dry ice bath under nitrogen protection.^[27] *n*-BuLi solution (0.8 mL, 1.25 mmol, 1.67 M in hexane) was added dropwise with stirring, after the addition the mixture was kept in a dry ice bath for 30 min and at RT for 30 min. The mixture was cooled in the dry ice bath and trimethyltinchloride solution (1.5 mL, 1.5 mmol, 1 M in hexane) was added, and the mixture was stirred at RT overnight. The mixture was quenched with water (50 mL) and extracted with hexane (50 mL) twice. The organic extraction was dried with anhydrous Na₂SO₄ and evaporated under vacuum. Recrystallization of the residue from isopropanol yielded compound **M1** as colorless needles (180 mg). Yield: 20.2%. ¹H NMR (500 MHz, CDCl₃, ppm): δ 7.51 (s, 2H), 4.30 (t, *J* = 7 Hz, 4H), 1.89 (m, 4H), 1.50 (m, 4H), 1.39-1.30 (m, 8H), 0.94 (t, *J* = 7 Hz, 6H), 0.45 (s, 18H). ¹³C NMR (500 MHz, CDCl₃, ppm): δ 165.4, 146.0, 145.4, 107.4, 73.8, 31.3, 22.2, 13.9, 3.4.

2,6-Bis(trimethylstannyl)-4,8-didecyloxybenzo[1,2-b:4,5-b']dithiophene (M2)

The same procedure as for compound **M1** was used. Compounds used were compound **4** (335 mg, 0.67 mmol), *n*-BuLi solution (1.1 mL, 1.66 mmol, 1.67 M in hexane), trimethyltinchloride solution (1.6 mL, 1.6 mmol, 1 M in hexane). Recrystallization of the residue from isopropanol yielded compound **M2** as colorless needles (122 mg). Yield: 25.1%. ¹H NMR (500 MHz, CDCl₃, ppm): δ 7.52 (s, 2H), 4.30 (t, *J* = 7 Hz, 4H), 1.89 (m, 4H), 1.58 (m, 4H), 1.40-1.29 (m, 20H), 0.89 (t, *J* = 7 Hz, 6H), 0.45 (s, 18H). ¹³C NMR (500 MHz, CDCl₃, ppm): δ 166.4, 146.4, 146.0, 102.0, 73.9, 31.9, 30.9, 29.6, 29.3, 26.1, 21.4, 14.1, 3.1.

5-Bromo-2-thiophenecarbaldehyde (5)

In ice-water bath, 2-thiophenecarboxaldehyde (2.24 g, 20 mmol) was put into a 50 mL flask, and the solution of 48% HBr (4.4 g, 26 mmol) was added into the flask dropwise within 10 min. Then, H₂O₂ (2.5 g, 23 mmol) was added dropwise into the flask at low temperature (5-15 °C) within 2 h and the solution was stirred intensively at RT for 8 h. The reaction was confirmed by thin layer chromatography. The reactant was poured into 13 mL of toluene and stirred for 10 min, and the organic layer was washed by deionized water (10 mL), NaHCO₃ solution (10 mL, 5% in water), Na₂SO₃ solution (5 mL, 5% in water), and deionized water (10 mL) successively. The crude product was purified by distillation under vacuum and compound **5** was collected as liquid product (2.8 g, 15.0 mmol). Yield: 75.2%. ¹H NMR (500 MHz, CDCl₃, ppm): δ 9.78 (s, 1H), 7.53 (d, *J* = 4 Hz, 1H), 7.20 (d, 1H). ¹³C NMR (500 MHz, CDCl₃, ppm): δ 181.7, 148.0, 139.2, 132.0, 120.1.

5-Bromo-2-thiopheneacetonitrile (6)

2-(2-Thienyl)-acetonitrile (2 g, 16.2 mmol) was dissolved in DMF (15 mL).^[29] After addition of NBS (2.9 g, 16.3 mmol), the reaction mixture was stirred at RT for 5 h. The crude mixture was poured into water (200 mL) and extracted with dichloromethane (100 mL) twice. Then the organic layer was dried over anhydrous MgSO₄. Finally, separation by means of silica-gel column chromatography (hexane: ethyl acetate =3: 1) gave a liquid product compound **6** (3.2 g, 15.9 mmol). Yield: 98.1%. ¹H NMR (500 MHz, CDCl₃, ppm): δ 6.55 (d, *J* = 4 Hz, 1H), 6.46 (d, *J* = 4 Hz, 1H), 3.6 (s, 2H). ¹³C NMR (500 MHz, CDCl₃, ppm): δ 132.3, 130.2, 126.9, 116.2, 112.2, 18.5.

Synthesis of (E)-2, 3-bis[2-(5-bromothieryl)]acrylonitrile (7)

Compound **5** (0.47 g, 2.5 mmol), compound **6** (0.50 g, 2.5 mmol) and sodium methoxide (0.13 g, 2.5 mmol) were added into a 50mL flask with methanol (20 mL). After the reaction mixture was stirred for 24 h at RT, the precipitate was filtrated. The crude product was purified by silica-gel column chromatography using methylene dichloride as an eluent. Compound **7** was obtained as a yellow solid (0.48 g, 1.3 mmol). Yield: 52%. ¹H NMR (500 MHz, CDCl₃, ppm): δ 7.27 (d, *J* = 4 Hz, 1H), 7.22 (s, 1H), 7.10-7.08 (m, 2H), 7.03 (d, *J* = 4 Hz, 1H). FT-IR (cm⁻¹): 3025, 2214, 1584, 1429, 1409, 1313, 905, 787, 500. ¹³C NMR (500 MHz, CDCl₃, ppm): δ 140.3, 139.2, 139.0, 132.7, 131.9, 127.9, 127.5, 120.1, 118.8, 117.1, 109.3.

Polymerization (Stille polycondensation)

PM1 and **PM2** were synthesized by coupling dibromo compounds and bis(trimethylstannyl) compounds.

Compound **7** (0.1mmol) was added into a 25 mL two-neck flask, and compound **M1** or **M2** (0.1 mmol) and Pd(PPh₃)₄ (22 mg, 0.02 mmol) were added. The flask was subjected to three successive cycles of vacuum followed by refilling with argon. Then, anhydrous DMF (1 mL) and anhydrous toluene (4 mL) were added via a syringe. The polymerization was carried out at 120 °C for 16 h under argon protection. The raw product was precipitated into methanol and collected by filtration. The precipitate was dissolved in CHCl₃ and reprecipitated in hexane. The solid was dried under vacuum for 12 h. The final polymer was purified by being washed with methanol and acetone in a Soxhlet Extractor for 24 h. After being dried, a dark brown solid was collected. The

yields of **PM1** and **PM2** were 40% and 50%, respectively.

2.3 Results and discussion

2.3.1 Synthesis and Characterization

The two target copolymers **PM1** and **PM2** were synthesized by the Stille polycondensation between the dibromo-functionalized precursor compound **7** and bis(trimethylstannyl)-substituted monomer (**M1** or **M2**) with a catalyst of Pd(PPh₃)₄ in toluene/DMF.^[30] The polymers were soluble in some common organic solvents such as THF, CHCl₃, and chlorobenzene at RT.

The structures of the copolymers were verified by ¹H NMR spectroscopy and FT-IR spectroscopy, all consistent with the propose ones. The complete disappearance of the proton signals of trimethylstannyl groups at 0.45 ppm for **M1** and **M2** confirms an efficient preparation of the target copolymers. It was found that signals of the oxy-methylene protons and side aliphatic protons appeared at 4.30 and 2.0-0.9 ppm, while the vinyl and aromatic protons signals appeared at 7.06-7.50 ppm. The FT-IR spectra showed sharp bands at 2210 cm⁻¹ (C≡N), 2924 cm⁻¹ (alkoxyl), and 1059 cm⁻¹ (CN-vinylene). As the inducement effect on the vinylene double bonds of the cyano group and the substituted groups linked to the backbone, the IR bands of the copolymers should appear around these areas, which confirmed the configuration of the target copolymers. GPC measurements revealed that the two copolymers have similar weight-averaged molecular weights of 19 and 23 kg mol⁻¹ with PDI of 2.1 and 2.4, respectively, which were summarized in Table 1. The molecular weight of a conjugated

polymer is known to affect the device performance of PSC ^[31] and the GPC results indicate that our polymers with moderate molecular weights are suitable for devices fabrication.

2.3.2 Thermal Properties

The thermal properties, an important factor for photovoltaic application, were measured by TGA. Fig. 2.2 depicts the TGA curves of copolymers **PM1** and **PM2**. They showed thermal decomposition temperatures (5% weight loss) of 343 and 339 °C for **PM1** and **PM2** under nitrogen, respectively. A slight decrease in the thermal stability from **PM1** to **PM2** is likely to be caused by the different lengths of alkoxy chains introduced into the BDT unit. Obviously, the two copolymers have adequate thermal stability for fabrication of PSCs and other optoelectronic devices.

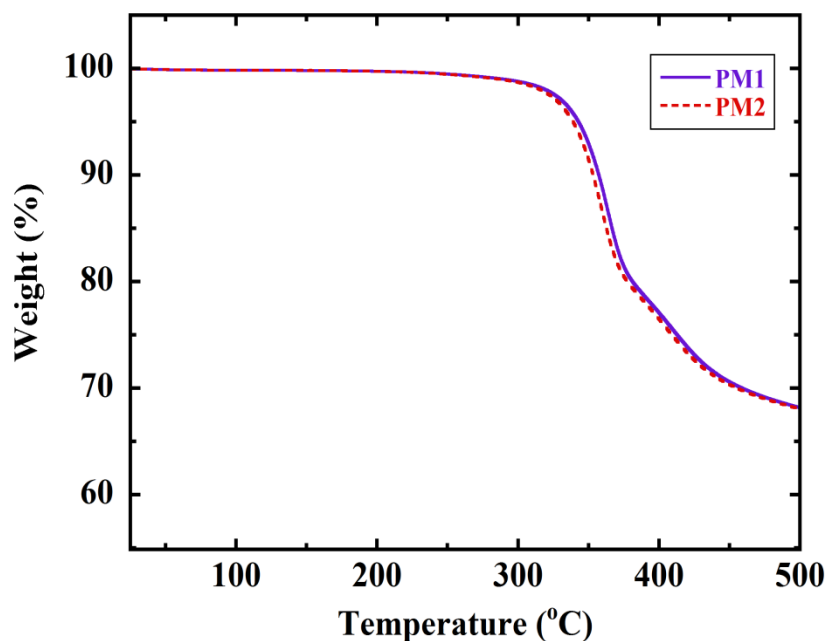


Fig. 2.2 TGA curves of **PM1** and **PM2** at a heating rate of 10 °C min⁻¹

under nitrogen.

Table 2.1 Thermal properties of **PM1** and **PM2**.

Polymer	M_n (kD) ^a	PDI	T_d (°C) ^b
PM1	19	2.1	343
PM2	23	2.4	339

^a Determined by GPC in THF based on polystyrene standards.

^b Decomposition temperature (with 5% weight loss) determined by TGA under N₂.

2.3.3 Optical Properties

The UV-vis absorption spectra of the copolymers in chloroform and in the solid film are shown in Fig. 2.3. The absorption maxima (λ_{\max}) of **PM1** and **PM2** in solution appeared at 500 and 509 nm, respectively. Compared with the solution spectra, the thin film absorption spectra of **PM1** and **PM2** were broadened and red-shifted by about 13 and 14 nm. We see a small hump at 620 nm in the film absorption spectra of **PM1** and **PM2**, indicating that a strong intermolecular interaction resulting in aggregation occurs in the solid state. The spectroscopic properties of **PM1** and **PM2** films are summarized in Table 2.2. The optical bandgap energies (E_g^{opt}) calculated from the onset absorption wavelengths (λ_{onset}) of the solid films were 1.85 eV (672 nm) for **PM1** and 1.83 eV (676 nm) for **PM2**. It has been reported that copolymers composed of a BTA unit combined with phenylenevinylene and didecyloxy naphthalene show bandgap energies of 2.10 and 1.89 eV, respectively.^[23,24] Our copolymers combining the BTA unit with a BDT unit

have bandgap energies smaller than the above copolymers due, most likely, to a planar conformation and strong interchain interactions caused by a smaller torsion angle between the D and A units.

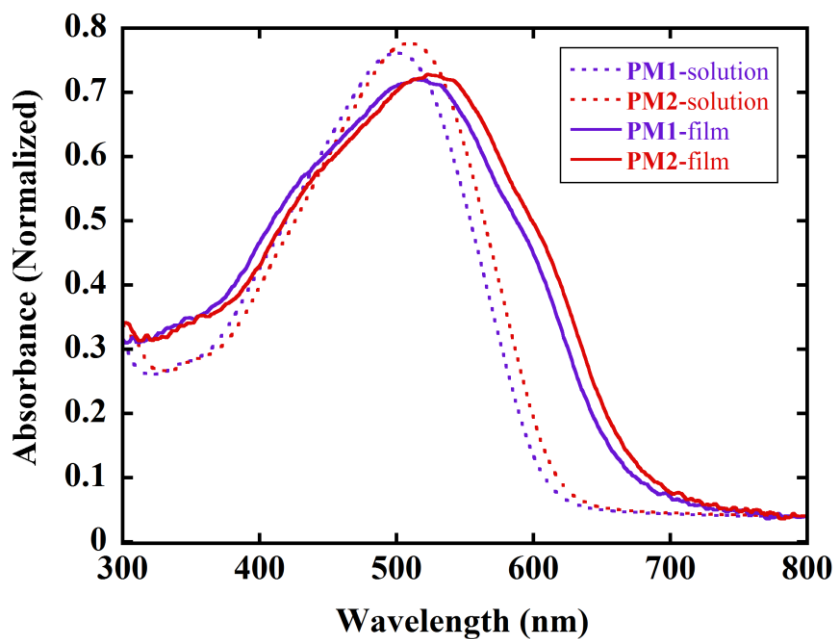


Fig. 2.3 UV-vis absorption spectra of **PM1** and **PM2** in chloroform (1.0×10^{-6} M) and in the solid film.

Table 2.2 Optical properties of **PM1** and **PM2** in solid state.

Polymer	λ_{\max} (nm)	λ_{onset} (nm)	E_g^{opt} (eV) ^a
PM1	513	672	1.85
PM2	523	676	1.83

^a $E_g^{\text{opt}} = 1240 / \lambda_{\text{onset}}$

2.3.4 Electrochemical Properties

Fig. 2.4 shows CVs of the two polymer films measured in TBAPF₆ (0.1 M)/CH₃CN solution under an argon atmosphere, where the potential was initially scanned at 50 mV s⁻¹ from 0 V to the anodic direction. The potential of Fc/Fc⁺ was measured in the same solution and found to be located at 0.04 V with respect to the Ag/Ag⁺ electrode. The onset oxidation potentials (E_{ox}) of **PM1** and **PM2** films were found to be 0.36 and 0.41 V vs. Fc/Fc⁺, respectively. The results indicate that the two copolymers possess high electron affinities, being attributed to the incorporation of double bonds and the cyano-substitution into the polymer backbone. The HOMO and LUMO energy levels of the copolymers films can be evaluated according to the following equations:^[32]

$$\text{HOMO} = -e(E_{ox} + 4.80) \text{ (eV)}$$

$$\text{LUMO} = \text{HOMO} + E_g \text{ (eV)}$$

where E_{ox} is the onset potential measured with respect to the redox potential of Fc/Fc⁺ and E_g is the bandgap of a polymer film, which was equated to E_g^{opt} calculated from the absorption spectrum. The electrochemical data are listed in Table 2.3 for comparison with the optical properties. From the optical and electrochemical data, the LUMO and HOMO energy levels were estimated to be about -3.31 and -5.16 eV for **PM1** and -3.38 and -5.21 eV for **PM2**, respectively. Although the chemical structures of these polymers are similar, the LUMO and HOMO levels of **PM2** are slightly lower than the corresponding energy levels for **PM1**. Energy band diagrams for the PSCs constructed in this study are illustrated in Fig. 2.5.

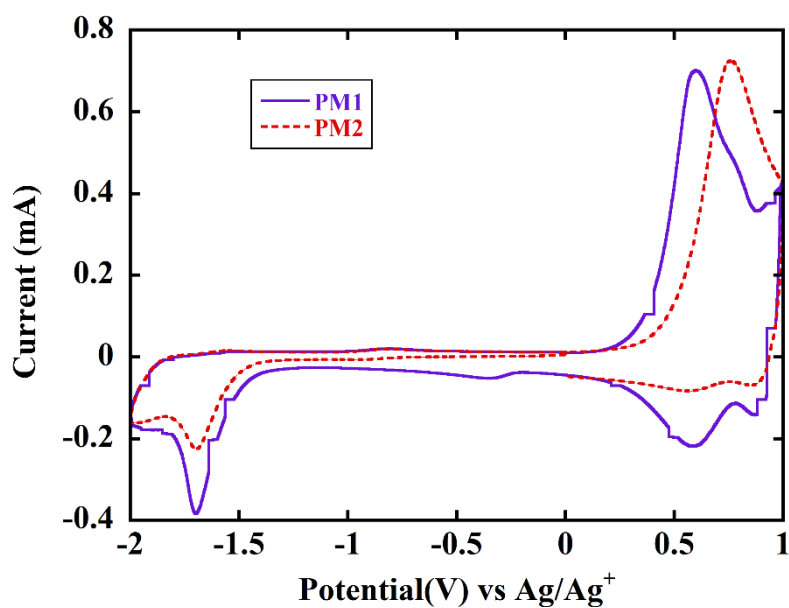


Fig. 2.4 Cyclic voltammograms of **PM1** and **PM2** films on Pt electrode in 0.1M TBAPF₆/CH₃CN solution at 50 mV s⁻¹.

Table 2.3 Electrochemical onset potentials and electronic energy levels of **PM1** and **PM2**.

Polymer	E_{ox} (V)	HOMO (eV)	LUMO (eV)
PM1	0.36	-5.16	-3.31
PM2	0.41	-5.21	-3.38

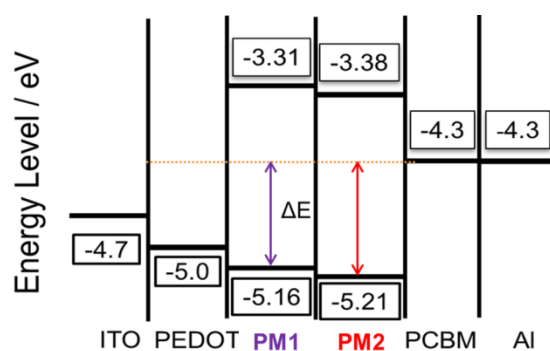


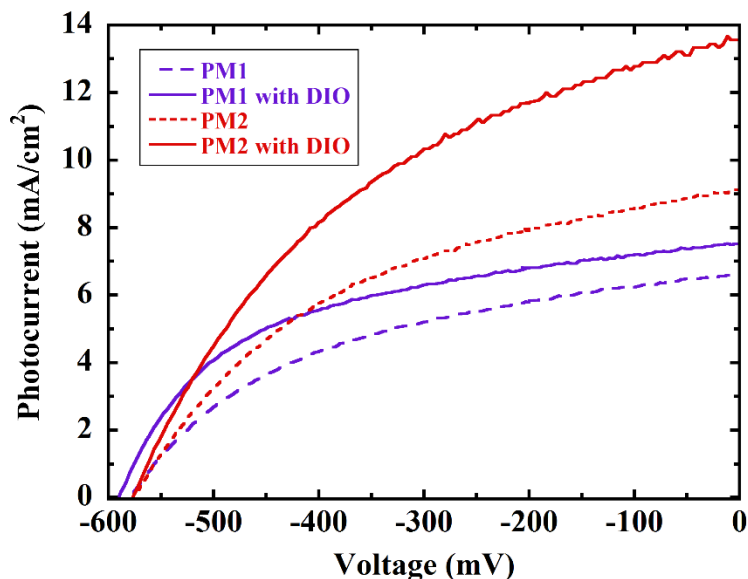
Fig. 2.5. Energy band diagrams for PSCs based on **PM1** and **PM2**.

Scharber et al. have reported a linear relationship between the HOMO level of the conjugated polymer and the V_{oc} of the PSC based on that polymer.^[7] In addition, they have illustrated the energy-conversion efficiency of the PSC as a function of E_g and the LUMO level of the donor polymer. According to this guideline, the V_{oc} s and PCEs of the PSCs based on **PM1** and **PM2** should be around 600 mV and 5%, respectively, when prepared under optimum conditions.

2.3.5 Photovoltaic Properties

The PSC devices based on the blends of the copolymers and PC₆₁BM were fabricated with a general device structure of ITO/PEDOT:PSS/polymer:PC₆₁BM(1:1, w/w)/LiF/Al. Fig. 2.6 shows photocurrent-voltage (J - V) curves of the PSCs and the photovoltaic parameters are summarized in Table 2.4. The PSCs based on **PM1** fabricated in air gave J_{sc} of 6.60 mA cm⁻², V_{oc} of 580 mV, modest FF of 45%, and PCE of 1.74%, while the device based on **PM2** gave a better performance with a higher J_{sc} of 9.23 mA cm⁻², similar V_{oc} of 580 mV, FF of 41%, and PCE of 2.20%. It has been reported that DIO is a very useful additive to enhance the performance of PSCs.^[33] In order to improve the device performance of our PSCs, we used chlorobenzene/DIO (97:3, v/v) as a solvent for preparing a blend solution of polymer/PC₆₁BM (1:1 w/w). As is shown in Table 4, an obvious increase of PCE was observed by using DIO for both **PM1** and **PM2**. The PCE of the **PM2** device with 3% DIO reaches 3.26% with V_{oc} of 580 mV, J_{sc} of 13.38 mA cm⁻², and FF of 42%. In the case of the **PM1** device, the PCE is 2.26% with V_{oc} of 588 mV, J_{sc} of 7.68 mA cm⁻², and FF of 50%. Compared with the

PSCs based on **PM1** and **PM2** without DIO, we can see that the FFs are still low for the PSCs with DIO. Dang and co-workers^[34] have found that the fabrication of devices in inert atmosphere gives higher FFs. By reference to their finding, we fabricated the devices of **PM2** in glovebox and measured their photovoltaic properties. As listed in Table 2.4, the V_{oc} increased slightly, and the FF gave a remarkable increase from 42 to 65%, although the J_{sc} decreased slightly. The PSCs thus prepared yielded a higher PCE (4.17%) than the others. It is obvious that the V_{oc} value of 600 mV and PCE value of 4.17% for our PSCs prepared under optimized conditions fit the reported guidance well.^[7] The incident photon-to-current conversion efficiency (IPCE) was measured as a function of wavelength of the incident monochromatic light. The IPCE spectrum for the PSC based on **PM2** is shown in Fig. 2.7. The IPCE spectrum is similar in shape to the absorption spectrum of the **PM2** film shown in Fig. 2.3, revealing that the polymer acts as a photoexcited electron donor.



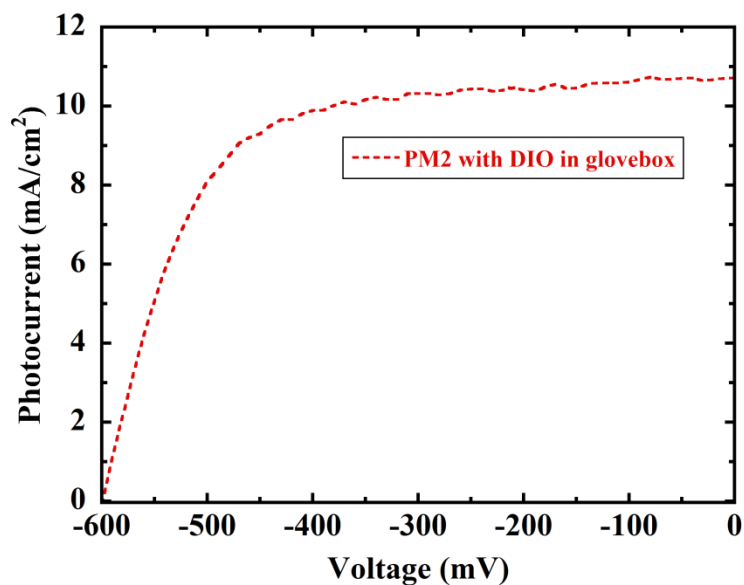


Fig. 2.6 (a) J - V curves of PSCs based on **PM1** or **PM2** with and without 3% DIO fabricated in air and (b) J - V curve of PSC based on **PM2** with 3% DIO fabricated in glovebox. J - V curves were measured under standard global AM 1.5 solar condition.

The performances of PSCs based on our polymers are better than those for other copolymers, reported earlier, composed of BTA and a donor unit: 0.01% for BTA-thienylenevinylene, 0.04% for BTA-phenylenevinylene, and 1.4% for BTA-naphthalene.^[23,24]

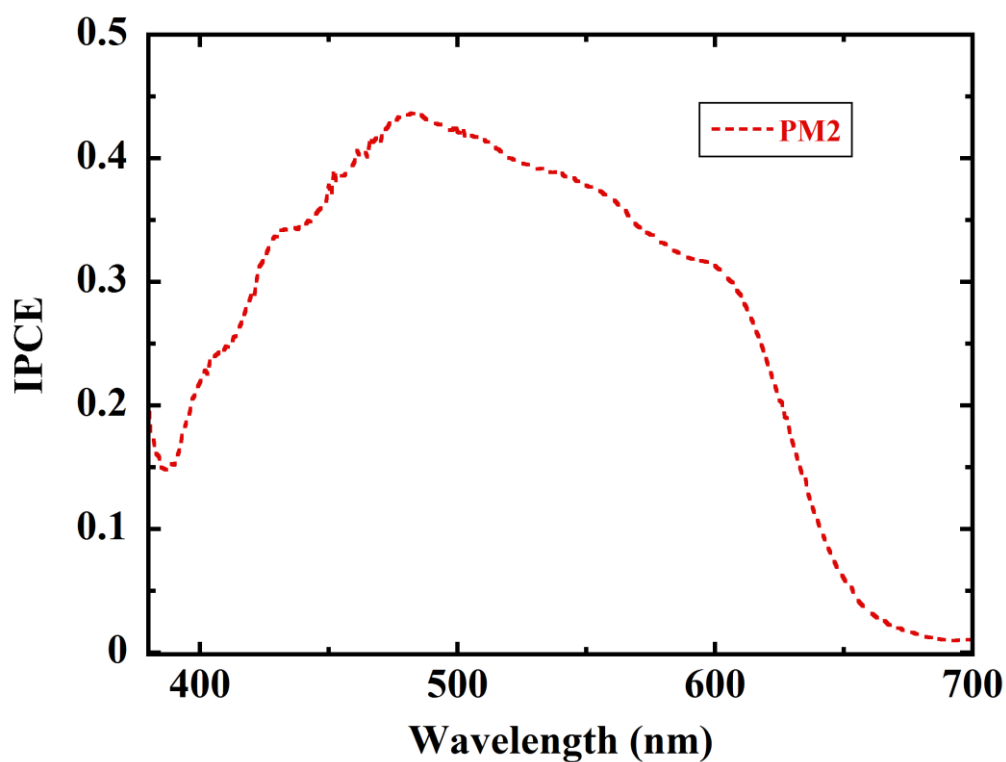


Fig. 2.7 IPCE spectrum of PSC based on **PM2**.

Table 2.4 Photovoltaic properties of PSCs based on **PM1** and **PM2** obtained under simulated solar light (AM 1.5, 100 mW cm⁻²).

Device ^a	additive	atmosphere	$J_{sc}/\text{mA cm}^{-2}$	V_{oc}/mV	FF/%	PCE/%
PM1	Non	Air	6.60	580	45	1.74
PM2	Non	Air	9.23	580	41	2.20
PM1	3% DIO	Air	7.68	588	50	2.26
PM2	3% DIO	Air	13.38	580	42	3.26
PM2	3% DIO	Argon	10.71	600	65	4.17

^a Polymer/PC₆₁BM (w/w) = 1:1

2.4 Conclusions

Two novel π -conjugated polymers (**PM1** and **PM2**) based on the combination of an electron-rich benzodithiophene (BDT) and an electron-deficient bithienylacrylonitrile (BTA) derivative were designed and synthesized for application to electron donor materials in polymer solar cells. The thermal, optical, and electrochemical studies showed that these two polymers had good thermal stability, broad absorption band in the visible range, and appropriate HOMO energy level, thus suitable for photovoltaic applications. The best PCE of the PSC based on **PM2**/PC₆₁BM/3%DIO reached 4.17%.

2.5 References and notes

1. S. B. Darling. *Energy Environ. Sci.*, 2009, **2**, 1266.
2. A. C. Mayer, S. R. Scully, B. E. Hardin, M. W. Rowell, and M. D. McGehee, *Mater. Today*, 2007, **10**, 28.
3. N. S. Sariciftci, L. Smilowitz, A. J. Heeger, and F. Wudl, *Science*, 1992, **258**, 1474.
4. S. Günes, H. Neugebauer, and N. S. Sariciftci, *Chem. Rev.*, 2007, **107**, 1324.
5. K. Colladet, S. Fourier, T. J. Cleij, L. Lutsen, J. G. D. Vanderzande, L. H. Nguyen, H. Neugebauer, N. S. Sariciftci, A. Aguirre, G. Janssen, and E. Goovaerts, *Macromolecules*, 2007, **40**, 65.
6. G. Yu, J. Gao, J. C. Hummelen, F. Wudl, and A. J. Heeger, *Science*, 1995, **270**, 1789.
7. M. C. Scharber, D. Muhlbacher, M. Koppe, P. Denk, C. Waldauf, A. J. Heeger, and C. J. Brabec, *Adv. Mater.*, 2006, **18**, 789.
8. D. Chirvase, Z. Chiguvare, M. Knipper, J. Parisi, V. Dyakonov, and J. C. Hummelenc, *J. Appl. Phys.*, 2003, **93**, 3376.
9. L. M. Campos, A. Tontcheva, S. Günes, G. Sonmez, H. Neugebauer, N. S. Sariciftci, and F. Wudl, *Chem. Mater.*, 2005, **17**, 4031.
10. C. Winder, and N. S. Sariciftci, *J. Mater. Chem.*, 2004, **14**, 1077.
11. Y. Sun, B. P. Lin, H. Yang, and X. H. Gong. *Polymer*, 2012, **53**, 1535.
12. M. Karakus, D. H. Apaydın, D. E. Yıldız, L. Toppare, and A. Cirpan. *Polymer*, 2012, **53**, 1198.
13. D. K. Susarova, E. A. Khakina, P. A. Troshin, A. E. Goryache, N. S. Sariciftci, V.

- F. Razumov, and D. A. M. Egbe. *J. Mater. Chem.*, 2011, **21**, 2356.
14. Y. M. Hwang, J. Ohshita, Y. Harima, T. Mizumo, Y. Ooyama, Y. Morihara, T. Izawa, T. Sugioka, and A. Fujita. *Polymer*, 2011, **52**, 3912.
15. H. A. Ho, H. Brisset, P. Frère, and J. Roncali. *J. Chem. Soc. Chem. Commun.*, 1995, **22**, 2309.
16. U. Schlick, F. Teichert, and M. Hanack. *Synth. Met.*, 1998, **92**, 75.
17. G. A. Sotzing, C. A. Thomas, and J. R. Reynolds. 1998, **31**, 3750.
18. C. A. Thomas, K. Zong, K. A. Abboud, P. J. Steel, and J. R. Reynolds. *J. Am. Chem. Soc.*, 2004, **126**, 16440.
19. H. A. Ho, H. Brisset, E. H. Elandalousi, P. Frère, and J. Roncali. *Adv. Mater.*, 1996, **8**, 990.
20. K. C. Li, Y. C. Hsu, J. T. Lin, C. C. Yang, K. H. Wei, and H. C. Lin. *J. Polym. Sci. Part. A: Polym. Chem.*, 2008, **46**, 4285.
21. M. X. Wan, W. P. Wu, G. Y. Sang, Y. P. Zou, Y. Q. Liu, and Y. F. Li. *J. Polym. Sci. Part. A: Polym. Chem.*, 2009, **47**, 4028.
22. J. H. Huang, K. C. Li, H. Y. Wei, P. Y. Chen, L. Y. Lin, D. Kekuda, H. C. Lin, K. C. Ho, and C. W. Chu. *Org. Electron.*, 2009, **10**, 1109.
23. J. A. Mikroyannidis, M. M. Stylianakis, K. Y. Cheung, M. K. Fung, and A. B. Djuricic. *Synth. Met.*, 2009, **159**, 142.
24. J. H. Kwon, J. Y. An, H. Jang, S. Choi, D. S. Chung, M. J. Lee, H. J. Cha, J. H. Park, C. E. Park, and Y. H. Kim. *J. Polym. Sci. Part. A: Polym. Chem.*, 2011, **49**, 1119.
25. H. Padhy, D. Sahu, D. Patra, M. K. Pola, J. H. Huang, C. W. Chu, K. H. Wei, and H. C. Lin. *J. Polym. Sci. Part. A: Polym. Chem.*, 2011, **49**, 3417.

26. J. H. Hou, M. H. Park, S. Q. Zhang, Y. Yao, L. M. Chen, J. H. Li, and Y. Yang. *Macromolecules*, 2008, **41**, 6012.
27. Y. Y. Liang, D. Q. Feng, Y. Wu, S. T. Tsai, G. Li, C. Ray, and L. P. Yu. *J. Am. Chem. Soc.*, 2009, **131**, 7792.
28. Z. Li, J. P. Lu, S. C. Tse, J. Y. Zhou, X. M. Du, Y. Tao, and J. F. Ding. *J. Mater. Chem.*, 2011, **21**, 3226.
29. J. W. Chung, H. Yang, B. Singh, H. Moon, B. K. An, S. Y. Lee, and S. Y. Park. *J. Mater. Chem.*, 2009, **19**, 5920.
30. B. Carsten, F. He, H. J. Son, T. Xu, and L. P. Yu. *Chem. Rev.*, 2011, **111**, 1493.
31. C. Nicolet, D. Deribew, C. Renaud, G. Fleury, C. Brochon, E. Cloutet, L. Vignau, G. Wantz, H. Cramail, M. Geoghegan, and G. Hadziioannou. *J. Phys. Chem. B.*, 2011, **15**, 12717.
32. Q. J. Sun, H. Q. Wang, C. H. Yang, and Y. F. Li. *J. Mater. Chem.*, 2003, **13**, 800.
33. J. K. Lee, W. L. Ma, C. J. Brabec, J. Yuen, J. S. Moon, J. Y. Kim, K. Lee, G. C. Bazan, and A. J. Heeger. *J. Am. Chem. Soc.*, 2008, **130**, 3619.
34. M. T. Dang, G. Wantz, L. Hirsch, and J. P. Parneix. *ECS. Transactions*, 2009, **23**, 449.

Chapter 3

Effects of π -conjugated side chains on properties and performances of photovoltaic copolymers

3.1 Introduction

In the past decade, polymer solar cells (PSCs) with a bulk-heterojunction (BHJ) structure have attracted many attentions as a potential renewable energy source due to advantages of low cost, light weight, easy fabrication, and capability to fabricate flexible devices.^[1-5] The BHJ structure with a nanoscale phase separation prepared by mixing a π -conjugated polymer as a p-type semiconductor and a fullerene derivative as an n-type semiconductor offers a high density of heterojunction interfaces responsible for the light-induced charge separation and thus produces a high power conversion efficiency (PCE).^[6-8] A number of studies have been devoted to the development of highly effective π -conjugated polymers applied in the BHJ photoactive layer. Soluble poly(3-alkylthiophene)s (PATs) are the most widely used π -conjugated polymers, but PATs have a drawback that they absorb light only in the range from 350 to 650 nm, although the solar spectrum ranges from 350 to 1500 nm with a maximum flux at around 700 nm. Alternating copolymers composed of electron donor (D) and electron acceptor (A) building blocks were designed to enhance the light-harvesting ability in terms of the intrachain charge transfer (ICT) absorption. Photophysical properties of D-A type copolymers can be fine-tuned by varying the electron-donating and

-withdrawing characteristics of the D and A building blocks, respectively. Many D-A copolymers have been synthesized and some of them have shown PCEs as high as 7-8%.^[9-14] According to this molecular-design concept, we have synthesized a D-A copolymer having a benzodithiophene (BDT) as a D unit and a bisthienylacrylonitrile (BTA) as an A unit (**PM2**), and obtained a reasonable PCE of 4.17%.^[15]

In most of the above-mentioned works, the side chains are used only to improve solubility of polymers or as a bridge to link with functional groups and there are few reports on the improvement of the conjugation of π -conjugated polymers through side chains. Undoubtedly, the expansion of the π -conjugation length will be desirable for improving various properties of polymers. In 1999, a series of phenyl-substituted polythiophenes was synthesized using FeCl_3 method.^[16] However, the large steric hindrance resulted in coplanarity of the polymer backbone because the phenyl ring was directly linked with the polymer backbone. To overcome this problem, some researchers introduced conjugated side-chains through vinylene ($\text{CH}=\text{CH}$) or acetylene ($\text{C}\equiv\text{C}$).^[17-22] Using this strategy, Li et al. synthesized polythiophenes with arylenevinylene side-chains, and succeeded in the improvement of light-harvesting ability because this type of polymers possesses two absorption peaks due to π - π^* transitions in both main and side chains.^[13] Furthermore, some research groups introduced the electron-withdrawing groups in the conjugated side-chains. In this molecular architecture, the side chains acted not only as a unit for enhancing light absorption but also as that for adjusting HOMO/LUMO energy levels in terms of ICT between the electron-donating polymer backbone and the electron-withdrawing side-chain.^[23-30]

In this report, we designed and synthesized three types of copolymers: a copolymer containing BDT and thiophene units in the main chain (no conjugated side-chain) (**PS0**),

PS0 containing a conjugated side-chain with no electron-withdrawing group (**PS1**), and **PS0** containing a BTA unit in the side chain, that is, a side chain unit containing a conjugated unit with an electron-withdrawing group (**PS2**). Optical, electrochemical, and photovoltaic properties of **PS0**, **PS1**, and **PS2** were studied and compared with those of a main chain type copolymer, **PM2**, to get an insight into the effect of the introduction of conjugated side-chain on photovoltaic properties of the conjugated copolymers.

3.2 Experimental

3.2.1 Materials

Bromo-2-ethylhexane, thiophene-2-yl-methanol, hydro-bromic acid (HBr, 47%), tetrakis(triphenylphosphine)palladium(0) ($\text{Pd}(\text{PPh}_3)_4$), triethylphosphite, potassium t-butoxide, and sodiummethoxide were purchased from Tokyo Chemical Industry. Diethylamine, trimethyltinchloride (1.0 M solution in hexane), 2,5-dibromothiophene, thiophene-3-carbaldehyde, and thiophen-2-yl-acetonitrile were purchased from Aldrich. n-Butyllithium(n-BuLi, 2.69 M solution in hexane) was purchased from Kanto Chemical. Co., INC. The reagents listed above were used without purification. N-Bromosuccinimide (NBS) and tetrabutylammoniumhexafluorophosphate (TBAPF_6) were purified by recrystallization. Tetrahydrofuran (THF), toluene, and acetonitrile (CH_3CN) were refluxed over CaH_2 , Na, and P_2O_5 , respectively, and then dis-tilled under nitrogen prior to use. N,N-Dimethylformamide (DMF) was distilled prior to use. Column chromatography was employed on silica gel 60N (spherical neutral).

Poly(3,4-ethylenedioxythiophene):poly(styrenesulfonate) (PEDOT:PSS, Clevious PH500) purchased from Heraeus Precious Metals GmbH & Co. KG was used after being filtrated through a 0.45 μm syringe filter (cellulose acetate). Likewise, a blend solution of polymer/PC₆₁BM (1:1, w/w, 15 mg/mL in chlorobenzene) was filtrated through a 0.20 μm syringe filter (PTFE).

3.2.2 Characterizations

NMR spectra were taken on a Varian 500 MHz instrument and chemical shifts were recorded in parts per million. The ultraviolet-visible (UV-vis) absorption spectra were measured using a Shimadzu UV-3150 spectrophotometer. Polymer molecular weights and polydispersity were determined by gel permeation chromatography (GPC) analysis using Shimadzu chromatograph with Shodex KF801, KF802, and KF803L columns at 40 °C with THF as eluent. Thermogravimetric analysis (TGA) was conducted with a SIC model TG/DTA-6200 at a heating rate of 10 °C/min under a nitrogen atmosphere, and differential scanning calorimetric (DSC) measurements were performed with a Shimadzu DSC-60 instrument at a scanning rate of 10 °C/min under a nitrogen atmosphere. Electrochemical measurements were performed at room temperature (RT) using a Hokuto Denko HSV-100 automatic polarization system under an argon atmosphere. A three-electrode cell equipped with a platinum sphere working electrode, an Ag/Ag⁺ (0.01 M in CH₃CN) reference electrode, and a platinum wire counter electrode was applied. All samples were measured in CH₃CN solutions containing 0.1 M TBAPF₆ as a supporting electrolyte. Ferrocene/ferrocenium redox couple (Fc/Fc⁺) was used as an internal reference. Atomic force microscopy (AFM) images of blend films

were recorded on an Agilent 5500 Scanning Probe Microscope instrument in the tapping mode.

3.2.3 Fabrication of PSCs and photovoltaic evaluations

The PSC devices were fabricated as described below. Indium-tin oxide (ITO) substrates were etched by a mixed acid solution (HCl:HNO₃:H₂O = 4:3:6) and then cleaned stepwise by ultrasonication in detergent, alkali solution, deionized water, acetone, and ethanol for 15 min for each. The cleaned ITO substrate was treated further with UV ozone for 30 min. A PEDOT:PSS buffer layer (about 30 nm in thickness) was formed on the ITO substrate by spin-coating and then heated on a hot plate at 100 °C for 10 min. Subsequently, in a glove box, a chlorobenzene solution of polymer/PC₆₁BM (1:1, w/w) with 1,8-diiodooctane (DIO, 3 vol%) was spin-coated on the PEDOT:PSS film and the blend film(100 nm) was annealed at 150 °C for 10 min. The PSC devices were completed by depositing LiF (0.6 nm) and Al (100 nm) as top electrodes with an area defined by a shadow mask (5 mm x 5 mm) under high vacuum ($< 2 \times 10^{-6}$ Torr) and annealed at 150 °C for 10 min. Photocurrent-voltage (J-V) characteristics were measured in an ambient atmosphere under the filtered light illumination from an Asahi HAL-302 solar simulator (AM 1.5 G, 100 mW/cm²). Data were recorded with a hand-made computer-controlled system. IPCE spectra were measured under a monochromatic irradiation with a tungsten halogen lamp and a monochromator.

3.2.4 Synthetic procedures

The synthetic routes of the monomers and copolymers are shown in Scheme 3.1.
2,6-Bis(trimethylstannyl)-4,8-bis(2-ethylhexyloxy)benzo[1,2-b:4,5-b']dithiophene

(M4) was synthesized according to a procedure reported previously.^[26] The detailed synthetic procedures of other compounds are described below.

2-Bromomethylthiophene (8)

2-Thienylmethanol 3 (1.91 mL, 20.2 mmol) was dissolved in anhydrous ether (50 mL) under a nitrogen atmosphere. HBr (47%, 3.42 mL) was added to the solution at 0 °C and the solution was kept at RT for 16 h. Then the solution was diluted with ice water (50 mL) and the aqueous layer was extracted with ether (2 x 25 mL). The combined organic extracts were washed with cold saturated NaHSO₄ solution until neutral pH and then washed with brine (50 mL). The organic phase was dried over anhydrous MgSO₄, filtered, and concentrated in vacuo to afford 2-bromomethylthiophene 4 as a pale greenish-yellow liquid. Yield: 3.23 g (90.15%). ¹H NMR (500 MHz, CDCl₃): δ (ppm) 7.33 (dd, J₁= 0.76 Hz, J₂= 5.11 Hz, 1H), 7.12 (d with fine coupling, J = 3.21 Hz, 1H), 6.95 (dd, J₁= 3.67 Hz, J₂= 4.94 Hz, 1H), 4.76 (s, 2H). ¹³C NMR (125 MHz, CDCl₃): δ (ppm) 136.14, 123.51, 122.28, 120.20, 29.49.

Diethyl(2-thienyl)methylphosphonate (9)

Under a nitrogen atmosphere, triethylphosphite (7.51 g, 40.1 mmol) and compound 4 (6.07 g, 34.0 mmol) were added into a 100 mL flask, and stirred at 125 °C. After 16 h, the produced bromoethane and the excess of triethylphosphite were removed under reduced pressure. The crude product was purified by vacuum distillation. A colorless oil of compound 5 was obtained. Yield: 6.42 g (80.81%). ¹H NMR (500 MHz, CDCl₃): δ (ppm) 7.18 (dd, J₁= 1.38 Hz, J₂= 5.10 Hz, 1H), 6.93 (dd, J₁= 0.78 Hz, J₂= 3.25 Hz, 1H), 6.89 (dd, J₁= 3.76 Hz, J₂= 4.80 Hz, 1H), 4.06 (t, J = 7.04 Hz, 4H), 3.39 (s, 2H), 3.34 (s,

2H), 1.23 (t, J = 7.06 Hz, 6H). ¹³C NMR (125 MHz, CDCl₃): δ (ppm) 137.75, 128.71, 127.83, 125.88, 63.12, 28.33, 16.18.

2,5-Dibromothiophene-3-carbaldehyde (10)

Thiophene-3-carbaldehyde 6 (4.52 g, 40.2 mmol) was dissolved in anhydrous DMF (40.00 mL) in a 100 mL flask under a nitro-gen atmosphere. NBS (16.10 g, 90.0 mmol) in anhydrous DMF (50.00 mL) was added dropwise to the mixture. The solution was stirred in the dark at RT overnight. The organic material was extracted with dichloromethane (DCM) and washed with deionized water. The extract was dried with anhydrous MgSO₄. After removing the solvent, the crude product was purified on chromatography using a hexane/DCM mixture (3:1 by volume) as eluent. Compound 7 was obtained as a yellow solid. Yield: 5.68 g, (52.89%). ¹H NMR (500 MHz, CDCl₃): δ (ppm) 9.79 (s, 1H), 7.34 (s, 1H). ¹³CNMR (125 MHz, CDCl₃): δ (ppm) 183.15, 139.28, 128.64, 124.21, 113.35.

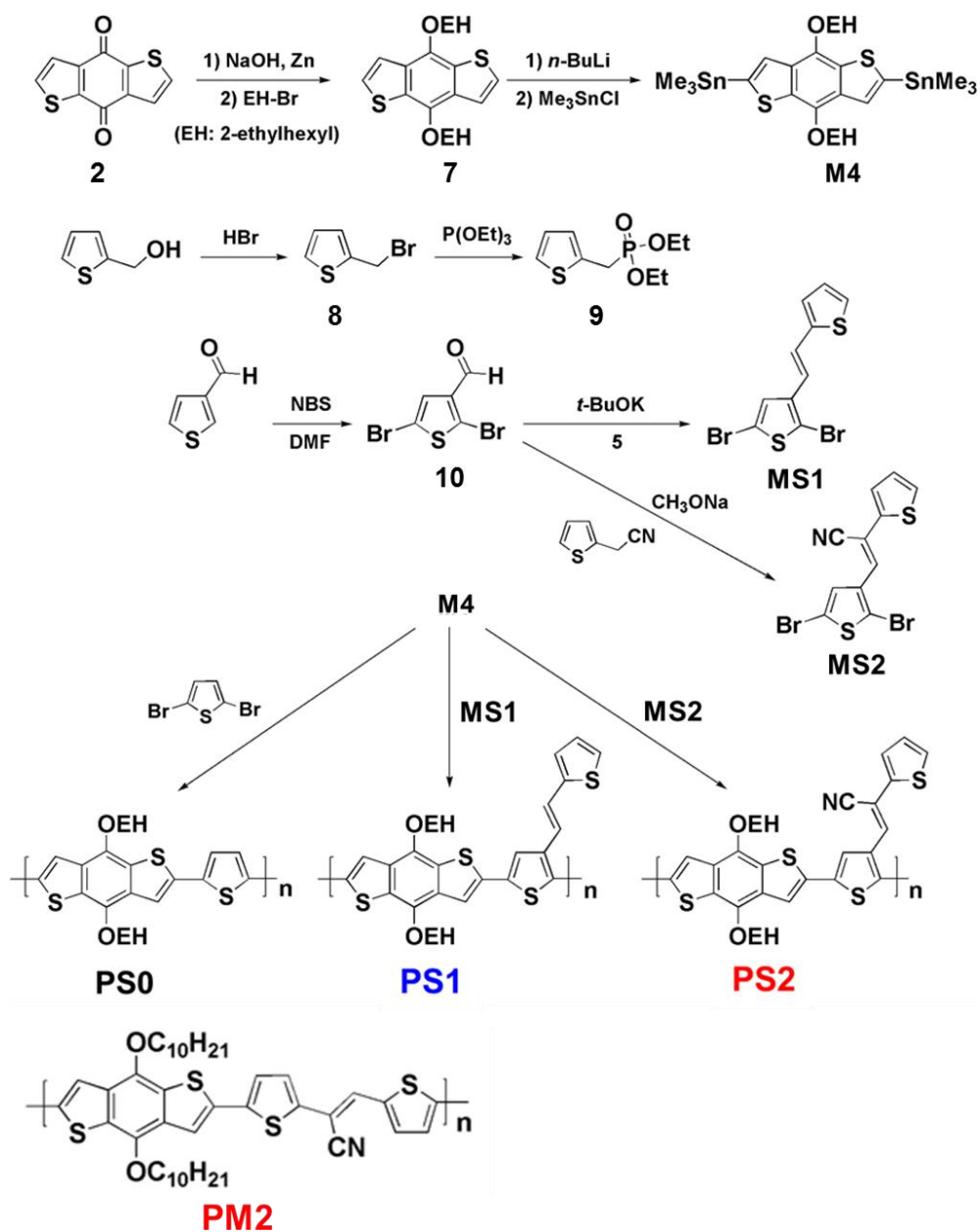
2,5-Dibromo-3-(2-(2-thienyl)-ethenyl)thiophene (MS1)

Potassium t-butoxide (11.25 mL, 1.0 M in THF) was added dropwise to the solution of compound 5 (1.17 g, 5.0 mmol) and compound 7 (1.35 g, 5.0 mmol) in THF (30 mL) at 0 °C. After being stirred at RT for 4 h, the mixture was poured into water and extracted with chloroform three times. The extract was dried with anhydrous MgSO₄. The solvent was removed by use of a rotary evaporator, and the residue was purified by recrystallization from methanol to get the compound M2 as a pale yellow solid. Yield: 1.21 g, (68.97%). ¹H NMR (500 MHz, CDCl₃): δ (ppm) 7.24 (d, J = 5.07 Hz, 1H), 7.16 (s, 1H), 7.08 (d, J = 3.30 Hz, 1H), 7.05-7.00 (m, 2H), 6.79 (d, J = 15.36 Hz, 1H). ¹³C

NMR (125 MHz, CDCl₃): δ (ppm) 141.92, 138.74, 127.74, 127.21, 126.81, 125.20, 124.32, 119.51, 111.91, 109.80.

3-(2,5-Dibromothiophen-3-yl)-2-thiophen-2-yl-acrylonitrile (MS2)

Compound 7 (0.67 g, 2.5 mmol), 2-(2-thienyl)acetonitrile (0.31 g, 2.5 mmol), and sodium methoxide (0.13 g, 2.5 mmol) were added to methanol (20 mL) in a 50 mL flask. After the reaction mixture was stirred for 24 h at RT, the precipitate was filtrated. The crude product was purified by silica-gel column chromatography using DCM as an eluent. Compound M3 was obtained as a yellow solid. Yield: 0.57 g, (61.29%). ¹H NMR (500 MHz, CDCl₃): δ (ppm) 7.94 (s, 1H), 7.40 (dd, J₁= 1.14 Hz, J₂= 3.69 Hz, 1H), 7.30 (dd, J₁= 1.15 Hz, J₂= 5.11 Hz, 1H), 7.28 (s, 1H), 7.09 (dd, J₁= 3.7 Hz, J₂= 5.10 Hz, 1H). ¹³C NMR (125 MHz, CDCl₃): δ (ppm) 138.50, 135.15, 129.42, 128.31, 127.88, 127.84, 126.96, 117.88, 116.25, 113.03, 106.87.



Scheme 3.1 Synthetic routes of **PS0**, **PS1**, and **PS2**, and chemical structure of **PM2**.

Polymerization (Stille polycondensation)

PS0, **PS1**, and **PS2** were synthesized by Stille coupling of dibromo compounds and bis(trimethylstannyl) compounds. **M1** (0.2 mmol) was added into a 25 mL two-neck flask, and 2,5-dibromothiophene or compound **M2** or **M3** (0.2 mmol) and Pd(PPh₃)₄ (46.2 mg, 0.04 mmol) were added. The flask was subjected to three successive cycles of

evacuation followed by refilling with argon. Then, anhydrous DMF (2 mL) and anhydrous toluene (8 mL) were added by using a syringe. The polymerization was carried out at 160°C for 16 h under an argon atmosphere. The raw product was precipitated into methanol. The precipitate was purified by being washed with methanol, hexane, and acetone by a Soxhlet Extractor for 24 h for each solvent. After being dried, the solid was collected.

PS0: reddish-brown color, yield (60.2 mg, 57.13%). ¹H NMR (500 MHz, CDCl₃): δ (ppm) 7.46-7.05 (br, 4H), 4.05 (m, 4H), 1.81-1.25 (m, 18H), 0.90 (br, 12H).

PS1: dark red color, yield (96.0 mg, 76.19%). ¹H NMR (500 MHz, CDCl₃): δ (ppm) 7.46-7.04 (br, 8H), 4.14 (m, 4H), 1.87-1.25 (m, 18H), 1.08 (br, 12H).

PS2: purple brown color, yield (92.0 mg, 70.19%). ¹H NMR (500 MHz, CDCl₃): δ (ppm) 7.68-7.10 (br, 7H), 4.21 (m, 4H), 1.85-1.24 (m, 18H), 0.89 (br, 12H).

3.3 Results and discussion

3.3.1 Synthesis and characterization

The three target copolymers **PS0**, **PS1**, and **PS2** were synthesized by the Stille polycondensation between bis(trimethylstannyl)-substituted monomer (M1) and the dibromo-functionalized precursors (2,5-dibromothiophene, M2, and M3) with a catalyst of Pd(PPh₃)₄ in toluene/DMF. The copolymers were soluble in common organic solvents such as THF, chloroform, and chlorobenzene at RT. Chemical structures of the copolymers were verified by ¹H NMR spectroscopy, all consistent with the proposed ones. The complete disappearance of the proton signals of H-C=O groups at 0.79 ppm

for compound 7 confirms an efficient preparation of the target monomers of M2 and M3. Likewise, the complete disappearance of the proton signals of trimethylstannyl groups at 0.45 ppm for M1 confirms an efficient preparation of the target copolymers. GPC measurements have revealed that the three copolymers have number-averaged molecular weights (M_n) of 0.97×10^4 , 4.4×10^4 , and 1.6×10^4 g/mol with PDI of 1.75, 3.40, and 1.44, respectively. The results are summarized in Table 1. The molecular weight of a conjugated polymer is known to affect the device performance of PSC^[31] and the GPC results indicate that our copolymers with moderate molecular weights are suitable for the fabrication of PSCs.

3.3.2 Thermal properties

The thermal property is one of the most important factors in photovoltaic applications of π -conjugated polymers because the poor thermal stability will cause the degradation of the active layer and the deformation of the polymer morphology at elevated temperatures. The thermal stability of the three copolymers was investigated with TGA and DSC. As shown in Fig. 3.1 and Table 3.1, the decomposition temperature at 5% weight loss (T_d) were 298, 317, and 276 °C for **PS0**, **PS1**, and **PS2**, respectively. **PS1** exhibited a little higher T_d than **PS0** and **PS2** due to a higher molecular weight of **PS1**, while the glass transition temperatures (T_g) of **PS0**, **PS1**, and **PS2** were 102, 143, and 153 °C, respectively. It is quite likely that the T_g values of **PS1** and **PS2** are much higher than that of **PS0** because the presence of conjugated side-chains hindered the molecular motion of the polymer backbone. In addition, the cyano group with high polarity is likely to enhance interactions between the polymer chains,^[22] leading to T_g of

PS2 being higher than that of **PS1**. Here, sufficiently high T_d values and reasonable T_g values indicate that the thermal stabilities of all copolymers are suitable for the fabrications of PSCs and other optoelectronic applications.

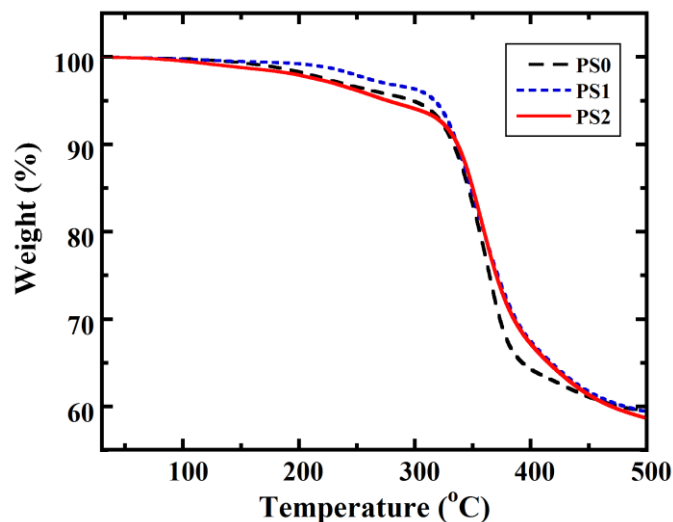


Fig. 3.1 TGA curves of **PS0**, **PS1**, and **PS2**.

Table 3.1

Molecular weights and thermal properties of **PS0**, **PS1**, and **PS2**.

	M_n (g/mol) ^a	M_w (g/mol) ^a	PDI ^a	T_d (°C) ^b	T_g (°C) ^c
PS0	0.97×10^4	1.7×10^4	1.75	298	102
PS1	4.4×10^4	15×10^4	3.40	317	143
PS2	1.6×10^4	2.3×10^4	1.44	276	153

^a Number average molecular weight (M_n) and weight average molecular weight (M_w) and polydispersity (PDI) of the copolymers were determined in THF by GPC using polystyrene standards.

^b 5% Weight loss temperature measured by TGA.

^c Determined by DSC.

3.3.3 Optical properties

The optical properties of the copolymers were investigated by measuring their UV-vis absorption spectra in chloroform and in the film state. The results are depicted in Fig. 3.2, together with the spectrum of **PM2** for a comparison. Here, absorbances of copolymers in solution are represented by those per repeat unit. **PS0** in solution shows a main absorption band at 500 nm with a vibronic structure, which is ascribable to π - π^* transition in the polymer backbone. In contrast, **PS1** shows a similar band at around 500 nm and an additional band at around 350 nm. The spectrum of **PS2** is similar to that of **PS1** and has two absorption bands, although the absorption intensity of the 350-nm band is higher than that of **PS1**. Since the wavelengths of these bands agree well with those for the corresponding monomers (M2 and M3) (Fig. 3.3), we presume that these additional bands at around 350 nm for **PS1** and **PS2** may be ascribed to the π - π^* transition in the localized π -conjugated system (the side-chain unit) and the introduction of a cyano group into side-chain enhanced the absorption intensity for **PS2** compared to **PS1**. On the other hand, **PM2** shows only one broad band in the wavelength range between 400 and 600 nm, which arises from a strong ICT between the electron-donating BDT and the electron-accepting BTA units in the main chain. In contrast, the side-chain copolymer **PS2** shows two absorption bands due, most likely, to the π - π^* transition in the side chain and a partial ICT between the conjugated side-chain with the electron-withdrawing cyano group and the BDT unit in the main chain. These results reveal that the introduction of conjugated side-chains enhances the light harvesting

ability compared with **PS0** and **PM2**. Compared with the solution spectra, the absorption spectra of copolymer films were broadened and red-shifted due to the intermolecular interaction caused by the aggregation in the solid state. The optical bandgap energies (E_{optg}) calculated from the onset absorption wavelengths (onset) of the solid films were 2.01 eV (615 nm) for **PS0**, 1.96 eV (633 nm) for **PS1** and 1.90 eV (650 nm) for **PS2**.

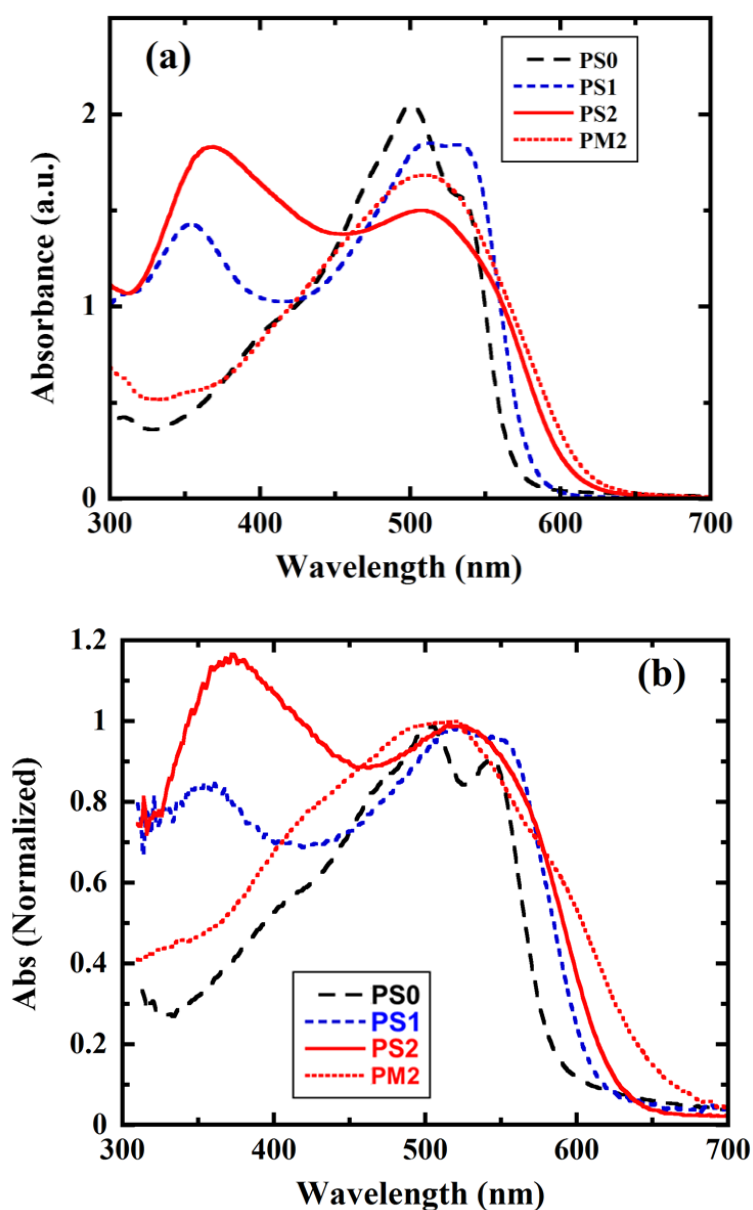


Fig. 3.2 UV-vis absorption spectra of **PS0**, **PS1**, **PS2** and **PM2** in chloroform (a) and in

the film state (b).

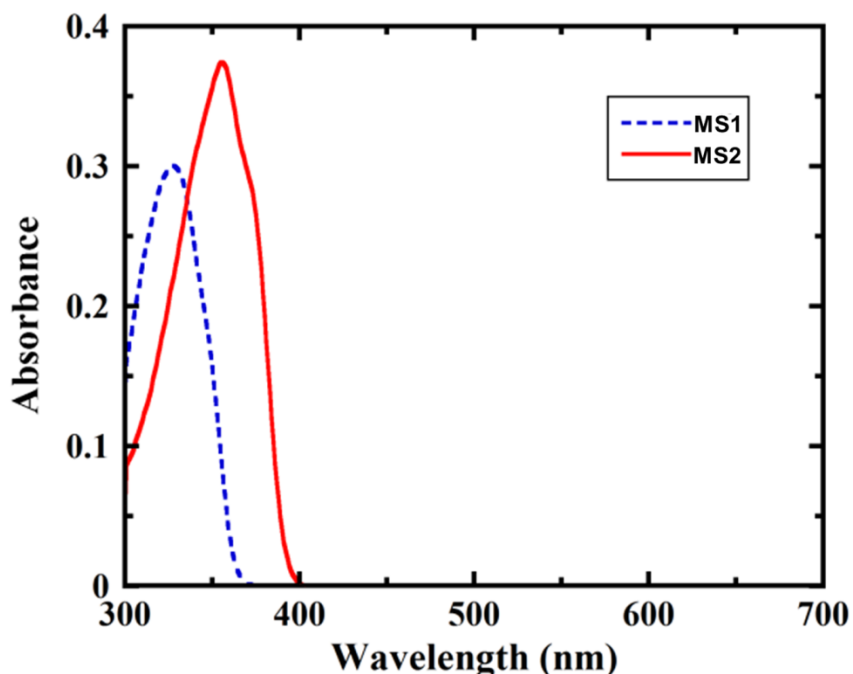


Fig. 3.3 UV-vis absorption spectra of MS1 and MS2 in chloroform. Measurements are made for the same concentrations of the solutions.

3.3.4 Electrochemical properties

Fig. 3.4 depicts CVs of the three copolymer films measured in TBAPF6 (0.1 M)/CH₃CN solution under an argon atmosphere, where the potential was scanned at 50 mV/s from 0 V to the anodic direction and switched back at +2.0 V. The half-wave potential of Fc/Fc⁺ was measured in the same solution and found to be located at 0.08 V with respect to the Ag/Ag⁺ electrode. The onset oxidation potentials (E_{ox}) of **PS0**, **PS1**, and **PS2** films were found to be 0.42, 0.42 and 0.57 V vs. Fc/Fc⁺, respectively. The results indicate that **PS2** possess a greater ionization potential than **PS0** and **PS1** due,

most likely, to the introduction of a cyano group. The HOMO and LUMO energy levels of the copolymer films were evaluated by using the following equations:^[32]

$$\text{HOMO} = -e (E_{\text{ox}} + 4.80) \text{ (eV)} \quad (1)$$

$$\text{LUMO} = \text{HOMO} + E \text{ (eV)} \quad (2)$$

where E_{ox} is the onset potential measured with respect to the half-wave potential of Fc/Fc⁺ and E_{optg} is the bandgap of a copolymer film calculated from the absorption spectrum. The electrochemical data are listed in Table 3.2. The LUMO and HOMO energy levels were estimated to be -3.21 and -5.22 eV for **PS0**, -3.26 and -5.22 eV for **PS1**, and -3.47 and -5.37 eV for **PS2**, respectively. The HOMO energy level of -5.37 eV for **PS2** lower than those of -5.22 eV for **PS0** and **PS1** is likely to be attributed to the donor-acceptor (D-A) effect between the polymer main chain and the pendant cyano group. Subsequently, the lower HOMO energy level and narrower bandgap caused the lower LUMO energy level for **PS2** compared to **PS0** and **PS1**. Energy band diagrams for the PSCs constructed in this study are illustrated in Fig. 3.5. It is seen from Fig. 5 that the energy levels of the three copolymers match the conditions for the efficient generation of photocurrents in the PSC configuration: the LUMO levels of the copolymers lie above the one of PC₆₁BM and the HOMO levels of the copolymers lie below the one of PEDOT-PSS.

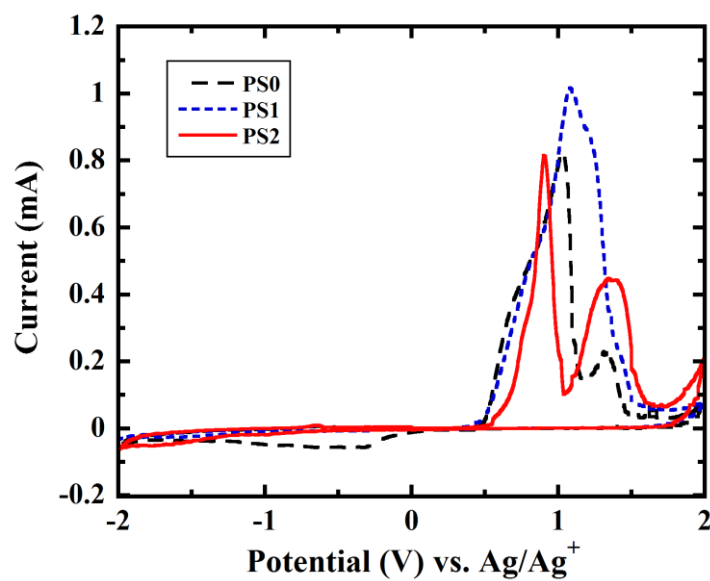


Fig. 3.4 Cyclic voltammograms of **PS0**, **PS1**, and **PS2** films on Pt electrode in TBAPF6(0.1 mol/L)/CH3CN solution at a scan rate of 50 mV/s.

Table 3.2

Optical and electrochemical properties of **PS0**, **PS1**, **PS2**, and **PM2** in solid state.

	λ_{\max} (nm)	λ_{onset} (nm)	E_g^{opt} (eV)	E_{ox} (V)	HOMO (eV)	LUMO (eV)
PS0	505	615	2.01	0.42	-5.22	-3.21
PS1	518	633	1.96	0.42	-5.22	-3.26
PS2	526	650	1.90	0.57	-5.37	-3.47
PM2	523	676	1.83	0.41	-5.21	-3.38

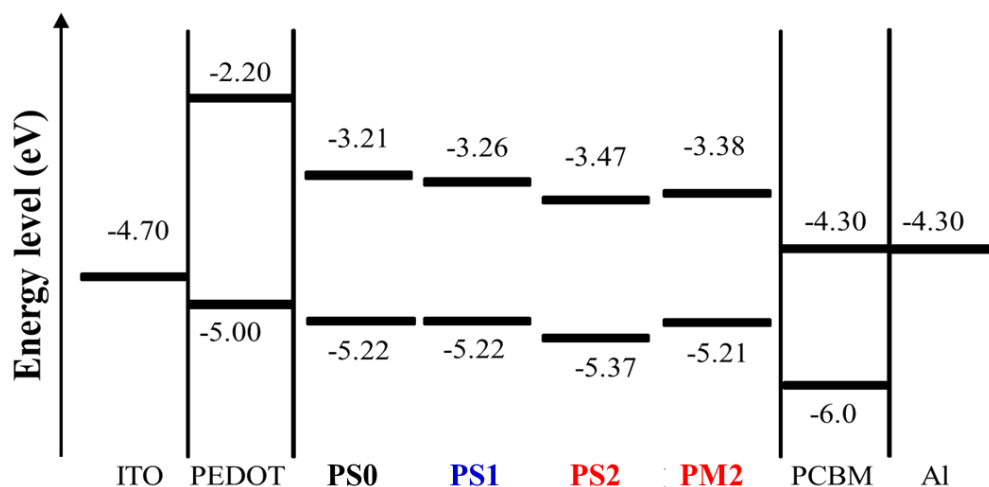


Fig. 3.5 HOMO and LUMO energy levels of **PS0**, **PS1**, **PS2**, and **PM2**.

3.3.5 Photovoltaic properties

PSC devices with a configuration of ITO/PEDOT:PSS/polymer:PC₆₁BM(1:1, w/w)/LiF/Al were constructed to evaluate photovoltaic properties of the copolymers designed and synthesized in this study. Fig. 3.6 shows the J - V curves of PSCs based on **PS0**, **PS1**, and **PS2**, along with the one for **PM2**. Table 3 summarizes the photovoltaic parameters obtained from the J - V curves. In comparison with the V_{oc} of the device based on **PS0** (620 mV), V_{oc} values for **PS1** (640 mV) and **PS2** (730 mV) are increased by 20 and 110 mV, respectively. The largest V_{oc} for **PS2** can be explained in terms of the deepest HOMO energy level of **PS2** (-5.37 eV) among others (-5.22 eV). The J_{sc} values were increased in the following order: **PS0** (6.92 mA/cm²) < **PS1** (9.30 mA/cm²) < **PS2** (11.49 mA/cm²), in agreement with the decreasing order of their bandgap energies. The superior light-harvesting ability of **PS2** can be viewed also in the IPCE spectra (Fig. 3.7): the PSC based on **PS2** absorbs a wide wavelength range of a sun light in terms of

the two absorption bands due to the π - π^* transition in the side chain and a partial ICT between the conjugated side-chain (BAT unit) and the BDT unit in the main chain. This light harvesting nature of **PS2** can be responsible for larger photocurrents of **PS2** than **PM2**, although the bandgap energy of **PS2** is slightly greater than that of **PM2**. Contrary to the expectation that the introduction of π -conjugated side-chain improves the charge transport property of the film and results in larger FF values,^[13,18,24] the FF values were decreased in the following order: **PS0** (0.66) > **PS1** (0.58) > **PS2** (0.53). To clarify the reason for the difference in FF among the three copolymer films, we studied the morphologies of the blend films composed of the copolymers and PC₆₁BM by means of AFM (Fig. 3.8). **PS0** and **PS1**/PC₆₁BM films showed rough surfaces due to the phase separation between copolymer and PC₆₁BM, whereas the surface of the **PS2**/PC₆₁BM film was smooth, suggesting a homogeneous dispersion of **PS2** and PC₆₁BM. It has been reported that the homogeneous dispersion of polymer and PC₆₁BM tends to hamper the establishment of the charge-transport pathway in the active layer, thus leading to the lowering of FF because of the high resistivity of the blend film.^[33,34] The low FF value for **PS2** may be explained on this basis. The PSC based on **PS2** showed the highest PCE of 4.49% compared with those of **PS0** (2.85%) and **PS1** (3.44%) due mainly to the largest V_{oc} and J_{sc} values. The PCE value of 4.49% for **PS2** is slightly larger than 4.17% for **PM2** in spite of the fact that the FF value of 0.53 for **PS2** is smaller than 0.65 for **PM2**. The results indicate that a side-chain copolymer can give a better photovoltaic performance than the corresponding main chain copolymer.

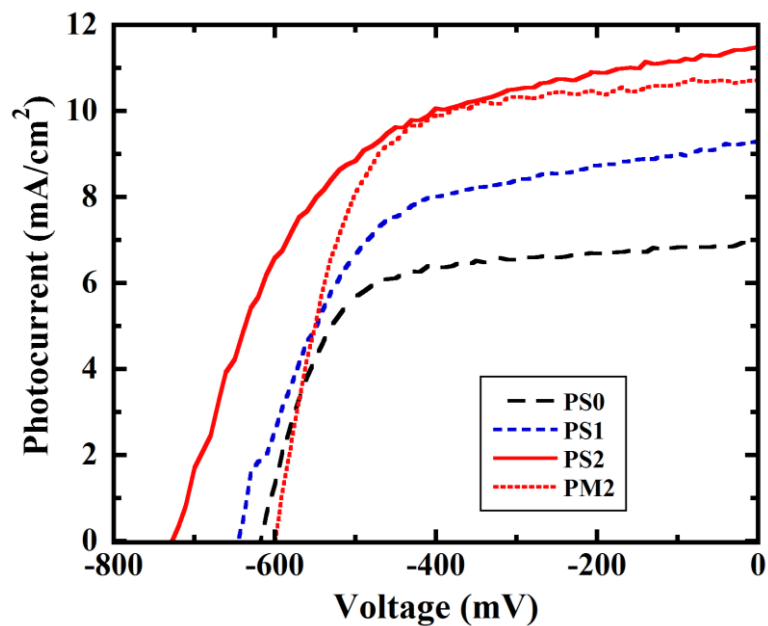


Fig. 3.6 J - V curves of PSCs based on PS0, PS1, PS2, and PM2.

Table 3.2

Photovoltaic performances of PSCs based on PS0, PS1, PS2, and PM2 (AM 1.5G, 100 mW/cm²).

	V_{oc} (mV)	J_{sc} (mA/cm ²)	FF	PCE (%)
PS0	620	6.92	0.66	2.85
PS1	640	9.30	0.58	3.44
PS2	730	11.49	0.53	4.49
PM2	600	10.71	0.65	4.17

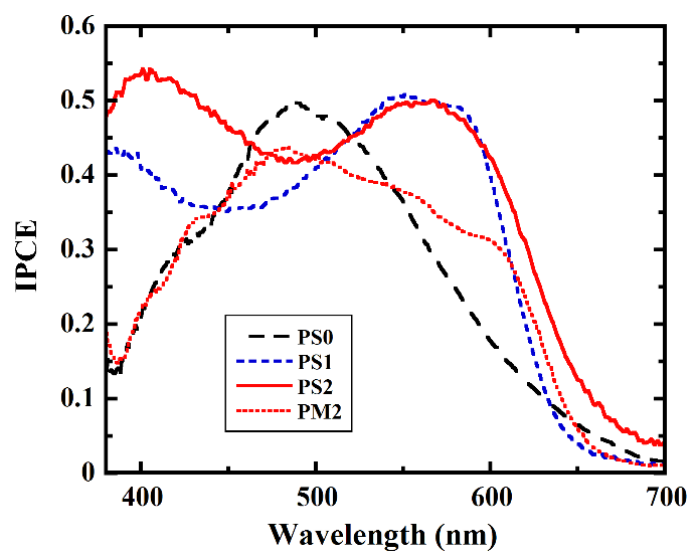


Fig. 3.7 IPCE spectra of PSCs based on **PS0**, **PS1**, **PS2**, and **PM2**.

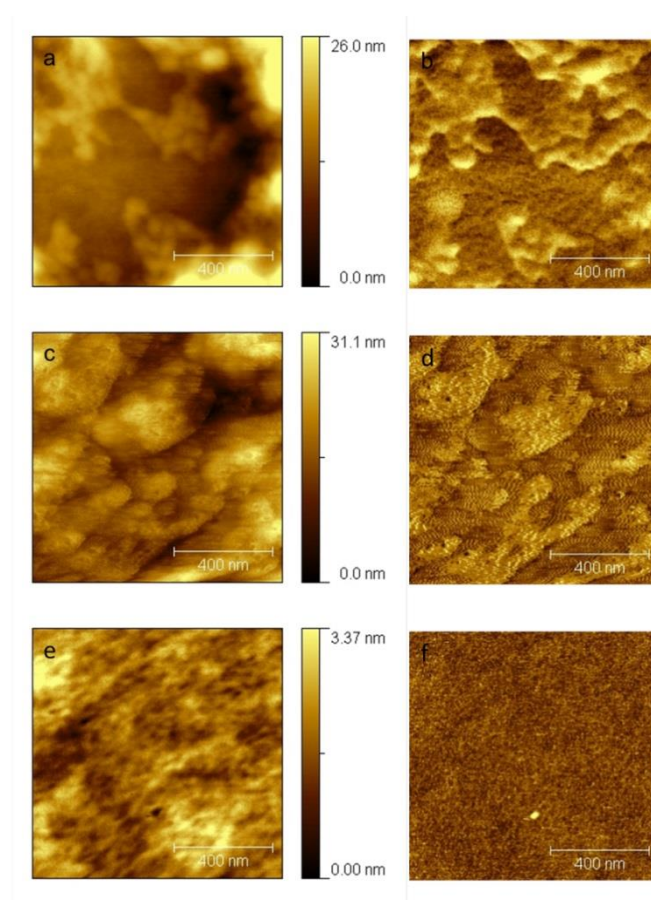


Fig. 3.8 Topographic (a, c, e) and phase (b, d, f) images of the blend films: **PS0/PC₆₁BM** (a, b), **PS1/PC₆₁BM** (c, d), and **PS2/PC₆₁BM** (e, f).

3.4 Conclusions

Three copolymers were designed and synthesized: a copolymer containing BDT and thiophene units in the main chain (**PS0**), **PS0** containing a conjugated side-chain with no electron-withdrawing group (**PS1**), and **PS0** containing a BTA unit in the side chain (**PS2**). These copolymers were soluble in common organic solvents and exhibited good film-forming abilities necessary for the device fabrication. The UV-vis spectra, electrochemical properties, and photovoltaic properties of the copolymer **PS2** were much improved in comparison with those of **PS0** and **PS1**. The PCE of PSC based on **PS2** reached 4.49% with V_{oc} of 730 mV, J_{sc} of 11.49 mA/cm², and FF of 0.53. These results indicate that modifying of the side chain can provide an effective method for designing high-performance D-A type photovoltaic copolymers.

3.5 References

1. N. S. Sariciftci, L. Smilowitz, A. J. Heeger, and F. Wudl, *Science*, 1992, 258 1474.
2. M. Y. Jo, J. H. Bae, G. E. Lim, Y. E. Ha, H. E. Katz, and J. H. Kim, *Synth. Met.*, 2003, **176**, 41.
3. K. Colladet, S. Fourier, T. J. Cleij, L. Lutsen, J. G. D. Vanderzande, L. H. Nguyen, H. Neugebauer, N. S. Sariciftci, A. Aguirre, G. Janssen, and E. Goovaerts, *Macromolecules*, 2007, **40**, 65.
4. G. Yu, J. Gao, J.C. Hummelen, F. Wudl, and A.J. Heeger, *Science*, 1995, **270** (1789).
5. H. A. Ho, H. Brisset, P. Frère, and J. Roncali, *J. Chem. Soc., Chem. Commun.*, 1995, **22**, 2309.
6. J. Min, Z. G. Zhang, S. Y. Zhang, and Y. F. Li, *Chem. Mater.*, 2012, **24**, 3247.
7. S. Günes, H. Neugebauer, and N. S. Sariciftci, *Chem. Rev.*, 2007, **107**, 1324.
8. S. W. Tsang, S. Chen, and F. So, *Adv. Mater.*, 2013, **25**, 2434.
9. Z. Zhang, Q. Peng, D. Yang, Y. Chen, Y. Huang, X. Pu, Z. Lu, Q. Jiang, and Y. Liu, *Synth. Met.*, 2013, **175**, 21.
10. J. M. Jiang, P. A. Yang, S. C. Lan, C. M. Yu, and K. H. Wei, *Polymer.*, 2013, **54**, 155.
11. H. L. Zhong, Z. Li, F. Deledalle, E. C. Fregoso, M. Shahid, Z. P. Fei, C. B. Nielsen, N. Yaacobi-Gross, S. Rossbauer, T. D. Anthopoulos, J. R. Durrant, and M. Heeney, *J. Am. Chem. Soc.*, 2013, **135**, 2040.
12. Y. Q. Yang, H. Park, S. H. Lee, D. H. Kim, and Y. S. Lee, *Synth. Met.*, 2013, **176**, 70.

13. J. H. Hou, Z. A. Tan, Y. Yan, Y. J. He, C. H. Yang, and Y. F. Li, *J. Am. Chem. Soc.*, 2006, **128**, 4911.
14. L. Dou, J. You, J. Yang, C. C. Chen, Y. He, S. Murase, T. Moriarty, K. Emery, G. Li, and Y. Yang, *Nat. Photonics*, 2012, **6**, 180.
15. Z. F. Tan, I. Imae, Y. Ooyama, K. Komaguchi, J. Ohshita, and Y. Harima, *Eur. Polym. J.*, 2013, **49**, 1634.
16. M. R. Andersson, W. Marnmo, T. Olinga, M. Svensson, M. Theander, and O. Ingantäs, *Synth. Met.*, 1999, **101**, 11.
17. P. Suresh, P. Balraju, G. D. Sharma, J. A. Mikroyannidis, and M. M. Stylianakis, *ACS Appl. Mater. Interfaces*, 2009, **1**, 1370.
18. E. J. Zhou, J. Z. Cong, K. Hashimoto, and K. Tajima, *Energy Environ. Sci.*, 2012, **5**, 9756.
19. E. J. Zhou, J. H. Hou, C. H. Yang, and Y. F. Li, *J. Polym. Sci., Part A: Polym. Chem.*, 2006, **44**, 2206.
20. H. J. Wang, J. Y. Tzeng, C. W. Chou, C. Y. Huang, R. H. Lee, and R. J. Jeng, *Polym. Chem.*, 2013, **4**, 506.
21. F. Huang, K. S. Chen, H. L. Yip, S. K. Hau, O. Acton, Y. Zhang, J. D. Luo, and A. K. Y. Jen, *J. Am. Chem. Soc.*, 2009, **131**, 13886.
22. E. Hittinger, A. Kokil, and C. Weder, *Angew. Chem. Int. Ed.*, 2004, **43**, 1808.
23. H. J. Wang, Y. P. Chen, Y. C. Chen, C. P. Chen, R. H. Lee, L. H. Chan, and R. J. Jeng, *Polymer*, 2012, **53**, 4091.
24. L. J. Huo, J. H. Hou, S. Q. Zhang, H. Y. Chen, and Y. Yang, *Angew. Chem. Int. Ed.*, 2010, **49**, 1500.

25. H. Y. Huang, Z. C. Cao, Z. J. Gu, X. W. Li, B. Zhao, P. Shen, and S. T. Tan, *Eur. Polym. J.*, 2012, **48**, 1805.
26. Z. G. Zhang, Y. L. Liu, Y. Yang, K. Y. Hou, B. Peng, G. J. Zhao, M. J. Zhang, X. Guo, E. T. Kang, and Y. F. Li, *Macromolecules*, 2010, **43**, 9376.
27. R. Kroon, A. Lundin, C. Lindqvist, P. Henriksson, T. Steckler, and M. Andersson, *Polymer*, 2013, **54**, 1285.
28. H. J. Fan, Z. G. Zhang, Y. F. Li, and X. W. Zhan, *J. Polym. Sci., Part A: Polym. Chem.*, 2011, **49**, 1462.
29. Y. P. Zou, G. Y. Sang, W. P. Wu, Y. Q. Liu, and Y. F. Li, *Synth. Met.*, 2009, **159**, 182.
30. Z. J. Gu, P. Tang, B. Zhao, H. Luo, X. Guo, H. J. Chen, G. Yu, X. P. Liu, P. Shen, and S. T. Tan, *Macromolecules*, 2012, **45**, 2359.
31. C. Nicolet, D. Deribew, C. Renaud, G. Fleury, C. Brochon, E. Cloutet, L. Vignau, G. Wantz, H. Cramail, M. Geoghegan, and G. Hadziioannou, *J. Phys. Chem. B*, 2011, **115**, 12717.
32. Q. J. Sun, H. Q. Wang, C. H. Yang, and Y. F. Li, *J. Mater. Chem.*, 2003, **13**, 800.
33. J. H. Kim, and S. G. Yim, *Appl. Phys. Lett.*, 2011, **99**, 193303.
34. B. Y. Qi, and J. Z. Wang, *Phys. Chem. Chem. Phys.*, 2013, **15**, 8972.

Chapter 4

Synthesis and electrical properties of novel oligothiophenes partially containing 3,4-ethylenedioxythiophenes

4.1 Introduction

Since 3,4-ethylenedioxythiophene (EDOT) has two electron-donating groups at the β -positions of thiophene ring, poly(3,4-ethylenedioxythiophene) (PEDOT) is electrochemically stable in the oxidation process and can show an excellent electrical conductivity.^[1] A water dispersion of its composite with poly(styrene sulfonate) (PEDOT-PSS) is commercially available and widely used in organic electronic devices such as organic photovoltaic cells and electroluminescent displays. PEDOT is known to be a mixture of oligomers ranging from six to eighteen units and has a poor solubility to common organic solvents.^[2] In the π -conjugated systems, it is known that a mixing of oligomers with different conjugation lengths causes unfavourable properties such as formation of trap-site for the charge transport,^[3] and dull color due to absorption of light over a wide wavelength region.^[4] Oligothiophenes have been studied as model compounds of polythiophenes and optical, electrochemical, and electrical properties of conducting polymers have been clarified through intensive studies with oligothiophenes.^[5-9] Because of their properties superior to those of polythiophenes due to the well-defined structures, numerous oligothiophenes have been synthesized^[10-12] and applied to the photo- and electroactive materials such as field-effect transistors,

electroluminescence and electrochromic displays, photovoltaic cells, and non-linear optics.^[13-20] Thus, if the EDOT-containing oligothiophenes with well-defined structure can be synthesized, the optoelectrical properties superior to PEDOT will be expected due to their uniform structure.

From this viewpoint, dimer,^[21,22] trimer,^[23,24] tetramer,^[25,26] and pentamer^[27] of EDOT were synthesized and their optical and electrochemical properties were investigated. However, EDOT oligomers longer than hexamer have not been synthesized yet, because of their poor solubility and instability in air. “Hybrid” oligothiophenes composed of EDOT and thiophene were synthesized to overcome this problem, and their optical, electrochemical, and electrical properties were investigated, but the longest oligothiophene which could be purely isolated was pentamer.^[28,29] Very recently, Nesterov et al. succeeded in the synthesis of hybrid octamer containing EDOT, but their research interest was not focused on the properties of oligothiophene themselves, but the electrochemical synthesis of EDOT containing polythiophenes using oligothiophenes as monomers.^[30]

In this study, we synthesize a series of EDOT-containing oligothiophenes (**EnTs**, $n = 3, 6, 7, 9, 11$) and investigate their optical and electrochemical properties in solution and the electrical properties in the solid film.

4.2 Experimental

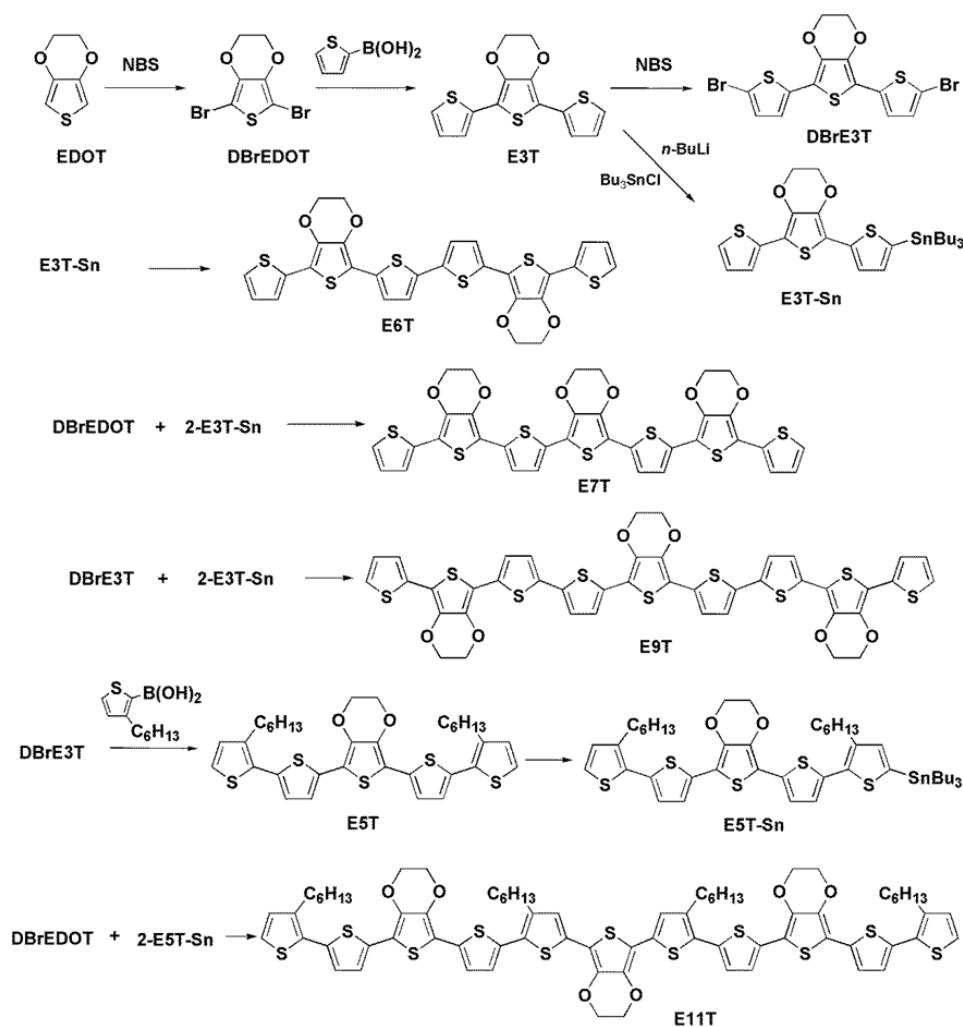
4.2.1 Materials

n-Hexane, toluene, tetrahydrofuran (THF), dichloromethane, and acetonitrile were

purified by standard methods and used immediately after purification. Tetraethylammonium perchlorate (TEAP) and *N*-bromosuccinimide (NBS) were purified by recrystallization from ethanol and benzene, respectively, and dried under vacuum. 3,4-Ethylenedioxythiophene (**EDOT**) and 3-hexyl-2-(4,4,5,5-tetramethyl-1,3,2-dioxaborolan-2-yl)thiophene (**HT-Bpin**) were purchased from Tokyo Chemical Industry and used without further purification. 2,5-Dibromo-3,4-ethylenedioxythiophene (**DBrEDOT**) and 3',4'-ethylenedioxy-2,2':5'',2''-terthiophene (**E3T**) were synthesized according to our previous report.^[31]

4.2.2 Synthesis

The synthetic routes of **EnTs** are shown in Scheme 4.1 and the detailed synthetic processes are described below.



Scheme 4.1 Synthesis of **EnTs** ($n = 3, 6, 7, 9, 11$). i) NBS/THF CH_3COOH ; ii) $\text{Pd}(\text{PPh}_3)_4$, $\text{Na}_2\text{CO}_3\text{aq}$ /THF; iii) NBS/ CHCl_3 - CH_3COOH ; iv) n -BuLi, Bu_3SnCl /THF; v) $\text{Pd}(\text{PPh}_3)_4$ /DMF

5,5''-Dibromo-3',4'-ethylenedioxy-2,2':5'',2''-terthiophene (DBrE3T).

To a $\text{CHCl}_3/\text{CH}_3\text{COOH}$ (20 mL/20 mL) solution of **E3T** (0.44 g, 1.43 mmol), a $\text{CHCl}_3/\text{CH}_3\text{COOH}$ (30 mL/30 mL) solution of NBS (0.51 g, 2.84 mmol) was slowly added at room temperature. The reaction mixture was stirred at a room temperature for 3 h. The reaction mixture was poured into water, and extracted two times with CHCl_3

(50 mL each). The combined organic extracts were washed with Na₂CO₃ aq and water and dried over Na₂SO₄. The solvent was removed by a rotary evaporator. **DBrE3T** (0.59 g, 1.27 mmol) was obtained as a yellow powder after column chromatography (SiO₂, *n*-hexane/toluene = 1/1 (v/v)), followed by recrystallization from *n*-hexane/dichloromethane. Yield: 89%. ¹H NMR (500 MHz, (CD₃)₂CO, δ, ppm): 4.49 (s, 4H, OCH₂CH₂O), 7.04 (d, *J* = 4.00 Hz, 2H, thienyl-**H**), 7.12 (d, *J* = 4.00 Hz, 2H, thienyl-**H**). MS (m/z): 461.80 (M⁺).

5-Tributylstannyl-3',4'-ethylenedioxy-2,2':5'',2''-terthiophene (E3T-Sn).

To a THF (10 mL) solution of **E3T** (0.10 g, 0.33 mmol), 0.2 mL of *n*-butyl lithium (1.65 M in *n*-hexane, 0.33 mmol) was added at 0 °C. After 1 h, tributyltin chloride (0.14 g, 0.42 mmol) was added in one portion. The reaction mixture was stirred at 0 °C for 1 h, then at room temperature for 1 h. After the solvent was removed by a rotary evaporator, *n*-hexane (50 mL) was added and the solution was stirred for 1 h. After filtration of the solution, the solvent was removed by a rotary evaporator. A dark red liquid was obtained. Product was used without further purification. ¹H NMR (500 MHz, (CD₃)₂CO, δ, ppm): 0.89 (t, *J* = 7.40 Hz, 9H, CH₃), 1.28 (t with fine coupling, *J* = 8.10 Hz, 6H, SnCH₂), 1.35 (tq, *J* = 7.40, 7.40 Hz, 6H, CH₂CH₃), 1.67 (tt, *J* = 7.40, 8.10 Hz, 6H, SnCH₂CH₂), 4.45 (s, 4H, OCH₂CH₂O), 7.05 (dd, *J* = 3.61, 5.14 Hz, 1H, thienyl-**H**), 7.15 (d, *J* = 3.43 Hz, 1H, thienylene-**H**), 7.26 (dd, *J* = 1.11, 3.61 Hz, 1H, thienyl-**H**), 7.38 (dd, *J* = 1.11, 5.14 Hz, 1H, thienyl-**H**), 7.39 (d, *J* = 3.43 Hz, 1H, thienylene-**H**).

3',4':3''',4''''-Bis(ethylenedioxy)-2,2':5'',2''':5''',2''''':5''''',2''''':5''''',2''''''-sexithiophene (E6T).

To a DMF (10 mL) solution of **E3T-Sn**, Pd(PPh₃)₄ (37 mg, 0.03 mmol) was added at room temperature. The reaction mixture after being stirred at 80 °C for 20 h was poured into distilled water (30 mL) and extracted with dichloromethane. The organic extract was washed with distilled water and dried over Na₂SO₄. The solvent was removed by a rotary evaporator. **E6T** (40 mg, 0.07 mmol) was obtained as a red solid after a column chromatography (SiO₂, *n*-hexane/toluene (1/2, v/v)). Yield: 40 %. ¹H NMR (500 MHz, CD₂Cl₂, δ, ppm): 4.42 (d with fine coupling, *J* = 2.57 Hz, 8H, OCH₂CH₂O), 7.05 (dd, *J* = 3.68, 5.07 Hz, 2H, thienyl-**H**), 7.12 (d, *J* = 3.88 Hz, 2H, thienylene-**H**), 7.14 (d, *J* = 3.88 Hz, 2H, thienylene-**H**), 7.25 (dd, *J* = 1.10, 3.68 Hz, 2H, thienyl-**H**), 7.26 (dd, *J* = 1.10, 5.07 Hz, 2H, thienyl-**H**). MS (m/z): 610.96 (M⁺).

3',4':3'',4''':3''''',4''''''-Tris(ethylenedioxy)-2,2':5',2'':5'',2''':5''',2''''':5''''',2''''''':5''''''',2''''''''- septithiophene (E7T).

E3T-Sn was prepared using **E3T** (0.50 g, 1.63 mmol). To a DMF (30 mL) solution of **E3T-Sn**, **DBrEDOT** (0.16 g, 0.53 mmol) and Pd(PPh₃)₄ (83 mg, 0.07 mmol) were added at room temperature. The reaction mixture after being stirred at 100 °C for 16 h was poured into Na₂CO₃ aq. The formed precipitate was collected by filtration, and washed by refluxed toluene (10 mL) to remove the starting materials and by-products. The remaining crude product was purified by recrystallization from distilled THF, and **E7T** (016 g, 0.21 mmol) was obtained as a red solid. Yield: 40 %. ¹H NMR (500 MHz, THF-*d*₈, δ, ppm): 4.41 (d with fine coupling, *J* = 3.42 Hz, 8H, OCH₂CH₂O), 4.43 (s, 4H, OCH₂CH₂O), 7.00 (dd, *J* = 3.60, 5.04 Hz, 2H, thienyl-**H**), 7.16 (s, 4H, thienylene-**H**), 7.23 (dd, *J* = 0.86, 3.60 Hz, 2H, thienyl-**H**), 7.30 (dd, *J* = 0.86, 5.04 Hz, 2H, thienyl-**H**). MS (m/z): 749.94 (M⁺).

**3',4':3''',4''':3''''''',4''''''''-Tris(ethylenedioxy)-2,2':5',2'':5'',2''':5''',2''''':5''''',
2''''':5''''',2''''''':5''''''',2''''''''':5''''''''',2''''''''''-novithiophene (E9T).**

E9T was prepared according to the same procedure as described for **E7T** by using **E3T** and **DBrE3T**. Yield: 31 %. ¹H NMR (500 MHz, (CD₃)₂SO, δ , ppm): 4.46 (d with fine coupling, $J = 6.90$ Hz, 8H, OCH₂CH₂O), 4.49 (s, 4H, OCH₂CH₂O), 7.09 (dd, $J = 3.61, 5.08$ Hz, 2H, thienyl-**H**), 7.19 (d, $J = 3.92$ Hz, 2H, thienylene-**H**), 7.20 (d, $J = 3.92$ Hz, 2H, thienylene-**H**), 7.25 (dd, $J = 1.04, 3.61$ Hz, 2H, thienyl-**H**), 7.31 (d, $J = 3.92$ Hz, 2H, thienylene-**H**), 7.32 (d, $J = 3.92$ Hz, 2H, thienylene-**H**), 7.52 (dd, $J = 1.04, 5.08$ Hz, 2H, thienyl-**H**). MS (m/z): 914.93 (M⁺).

3,4''''-Dihexyl-3'',4''-ethylenedioxy- 2,2':5',2'':5'',2''':5''',2''''-quinquethiophene (E5T).

E5T was prepared according to the similar procedure to our previous report for **E3T** by using **HT-Bpin** and **DBrE3T**. Yield: 24 %. ¹H NMR (500 MHz, (CD₃)₂CO, δ , ppm): 0.87 (t, $J = 7.21$ Hz, 6H, CH₃), 1.28-1.35 (m, 8H, (CH₂)₂CH₃), 1.35-1.42 (m, 4H, thienyl-(CH₂)₂CH₂), 1.66 (tt, $J = 7.21, 7.82$ Hz, 4H, thienyl-CH₂CH₂), 2.80 (t, $J = 7.82$ Hz, 4H, thienyl-CH₂), 4.50 (s, 4H, OCH₂CH₂O), 7.03 (d, $J = 5.20$ Hz, 2H, thienyl-**H**), 7.12 (d, $J = 3.91$ Hz, 2H, thienylene-**H**), 7.26 (d, $J = 3.91$ Hz, 2H, thienylene-**H**), 7.37 (d, $J = 5.20$ Hz, 2H, thienyl-**H**). MS (m/z): 638.15 (M⁺).

3,4''''-Dihexyl-5-tributylstannyl-3'',4''-ethylenedioxy-2,2':5',2'':5'',2''':5''',2''''-quinquethiophene 5 (E5T-Sn).

E5T-Sn was prepared according to the same procedure as described for **E3T-Sn** by

using **E5T**. ^1H NMR (500 MHz, $(\text{CD}_3)_2\text{CO}$, δ , ppm): 0.85-0.93 (m, 15H, CH_3), 1.17 (t with fine coupling, 6H, $J = 8.06$ Hz, SnCH_2), 1.27-1.46 (m, 18H, thienyl- $(\text{CH}_2)_2(\text{CH}_2)_3\text{CH}_3$ and $\text{Sn}(\text{CH}_2)_2\text{CH}_2\text{CH}_3$), 1.58-1.70 (m, 10H, thienyl- CH_2CH_2 and $\text{Sn}-\text{CH}_2\text{CH}_2$), 2.80 (t, $J = 0.98$ Hz, 4H, thienyl- CH_2), 4.50 (s, 4H, $\text{OCH}_2\text{CH}_2\text{O}$), 7.03 (d, $J = 5.20$ Hz, 1H, thienyl- H), 7.11 (s, 1H, thienylene- H), 7.12 (d, $J = 3.93$ Hz, 1H, thienylene- H), 7.12 (d, $J = 3.93$ Hz, 1H, thienylene- H), 7.26 (d, $J = 3.93$ Hz, 1H, thienylene- H), 7.26 (d, $J = 3.93$ Hz, 1H, thienylene- H), 7.37 (d, $J = 5.20$ Hz, 1H, thienyl- H).

3'',4'':3''''',4''''':3''''''',4''''''':-Tris(ethylenedioxy)-3,3''',4''''',3''''''''-tetrahexyl-2,2':5',2'':5'',2''':5''',2''''':5''''',2''''''':5''''''-undecithiophene (E11T).

E11T was prepared according to the same procedure as described for **E7T** by using **E5T** and **DBrEDOT**. Yield: 34 %. ^1H NMR (500 MHz, CD_2Cl_2 , δ , ppm): 0.89 (t, $J = 7.15$ Hz, 6H, CH_3), 0.91 (t, $J = 7.15$ Hz, 6H, CH_3), 1.30-1.50 (m, 24H, $(\text{CH}_2)_3\text{CH}_3$), 1.60-1.75 (m, 8H, thienyl- CH_2CH_2), 2.79 (t, $J = 7.83$ Hz, 8H, thienyl- CH_2), 4.43 (s, 12H, $\text{OCH}_2\text{CH}_2\text{O}$), 6.96 (d, $J = 5.19$ Hz, 2H, thienyl- H), 7.05 (d, $J = 3.79$ Hz, 2H, thienylene- H), 7.06-7.12 (m, 4H, thienylene- H), 7.18-7.22 (m, 6H, thienyl- H and thienylene- H). MS (m/z): 1415.27 (M^+).

4.2.3 Measurements

UV-Vis absorption spectra were taken on a spectrophotometer (Shimadzu, UV-3150). Cyclic voltammetry and spectroelectrochemistry were made in TEAP (0.1 M)-acetonitrile using a potentiostat/galvanostat (Hokuto Denko, HAB-151) and an X-Y

recorder (Riken Denshi, F-57). *In situ* conductivity measurements were made, also in TEAP (0.1 M)-acetonitrile, by using the two-probe method with a micro-array Pt electrode (ALS Co., Ltd, 65 lines, separation distance = 5 μm , total width = 260 μm) or with a two-band Pt electrode (homemade, separation distance = 100 μm , width = 7 mm).^[31-38] The amounts of charges generated by electrochemical oxidation (doping) and reduction (dedoping) of the **E11T** film were measured with a coulometer (homemade), where the potential was stepped from -0.5 V to a desired potential and back to -0.5 V, respectively. Doping levels, defined as the number of charges per thiophene ring, were estimated from the doping/dedoping charges, weight of **E11T** film, and molecular weight of the monomer unit. Apparent mobilities (μ) of charge carriers in **E11T** at various doping levels (electrode potentials) were calculated from the following relation, $\mu = \sigma/ne$, where σ , n , and e denote the electrical conductivity at an electrode potential, the density of charge carriers estimated from the doping/dedoping charges, and the elementary charge, respectively. Thicknesses and morphology of oligothiophene films were evaluated by a 3D laser microscope (Keyence Corp., VK-9700). Field-effect transistors using **E11T** were fabricated in a bottom-gate/top-contact configuration. An *n*-type heavily doped Si wafer with a SiO₂ layer of 200 nm and a capacitance of 14.1 nF cm⁻² was used as the gate electrode and dielectric layer. Before the deposition of **E11T** film, the gate dielectrics were placed in toluene solution of octyltrichlorosilane (OTS) to form an OTS self-assembled monolayer (SAM). Then the chloroform solution of **E11T** was spin-coated on the OTS-modified SiO₂/Si substrate. The device characteristics were measured in air and Argon by using Keithley 2400 and 2611 sourcemeters. The field-effect mobility was calculated in the saturation regime by using the equation, $I_{DS} = (W\mu C_i/2L)(V_{GS}-V_{th})^2$, where I_{DS} denotes the drain-source current, μ the field-effect

mobility, W is the channel width (1 mm), L the channel length (100 μm), C_i the capacitance per unit area of the gate dielectric layer, V_{GS} the gate voltage, and V_{th} is the threshold voltage.

4.3 Results and Discussion

4.3.1 Synthesis of Hybrid EDOT-Containing Oligothiophenes

A series of oligothiophenes partially containing EDOT was synthesized as described in Scheme 1. Terthiophene having one EDOT unit (**E3T**) was synthesized by the Suzuki-Miyaura coupling from 2-thiophene boronic acid and 2,5-dibromo-3,4-ethylenedioxythiophene in the reasonable yield.^[31] Using **E3T** as a key compound, hexamer (**E6T**), heptamer (**E7T**), and nonamer (**E9T**) were synthesized by the Stille-coupling. The solubility of EDOT-containing oligothiophenes was much higher than those of unsubstituted oligothiophenes, although the solubility decreased with the increase of the chain length of oligothiophenes due to the enhancement of their π - π interactions. When nonamer (**E11T**) was synthesized, four alkyl chains were introduced to increase the solubility. All compounds were characterized by ^1H NMR and mass spectroscopies.

4.3.2 Geometrical Effect of EDOT

To investigate the effect of the introduction of EDOT units into oligothiophenes, optical properties of **E3T** were compared with those of 2,2':5',2''-terthiophene (**3T**).

Fig. 4.1 shows the electronic absorption and emission spectra of **E3T** and **3T**. The absorption spectrum of **3T** showed a structureless peak due to the rotational freedom of thiophene rings, while the absorption band of **E3T** showed a well-resolved vibronic structure. The absorption maximum of **E3T** was observed at 374 nm, remarkably red-shifted from that of **3T** ($\lambda_{\text{max}} = 354$ nm), whereas emission spectra of **E3T** and **3T** were similar in shape to each other.

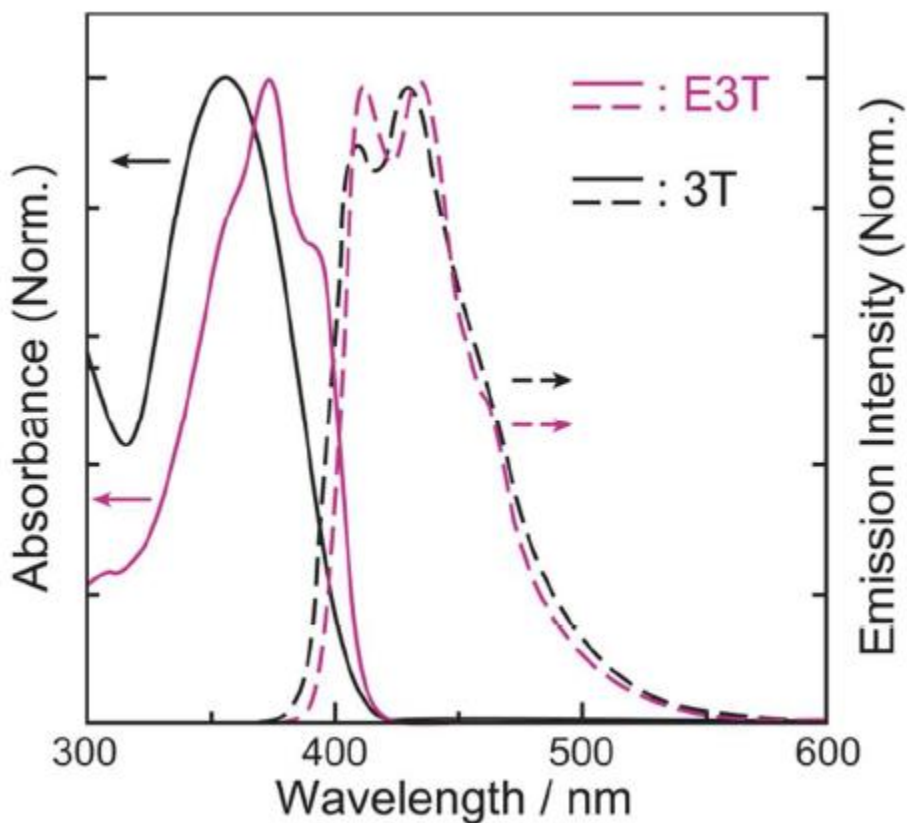


Fig. 4.1 Electronic absorption (solid) and emission (dashed) spectra of **E3T** (purple) and **3T** (black) in dichloromethane solution. For emissionspectra, excitation at 354 nm.

For understanding these results, we estimated the molecular structures of **E3T** and **3T** by *ab initio* MO method using Gaussian 09 (HF/6-31*, C_2 -symmetry) (Fig. 4.2). While

the dihedral angle of **3T** was around 30 degrees, that of **E3T** was almost 0 degree. Very recently, it is reported that the intramolecular interaction between chalcogen atoms affects the geometry of molecules, although the origin of the interaction is still not clear.^[39-43] For example, it is reported that the crystal structure of EDOT dimer shows the planar structure, and that the distances between sulfur and oxygen atoms is significantly shorter than the sum of their van der Waals radii, which evidences the occurrence of the above-mentioned strong interaction.^[39] Such a rigid conjugated system will cause the quinoid-like planar geometry even in ground state of **E3T**, which is likely to give the vibronic fine structure in the absorption spectrum and the decrease in the Stokes shift of the emission spectrum as observed in Fig. 4.1.

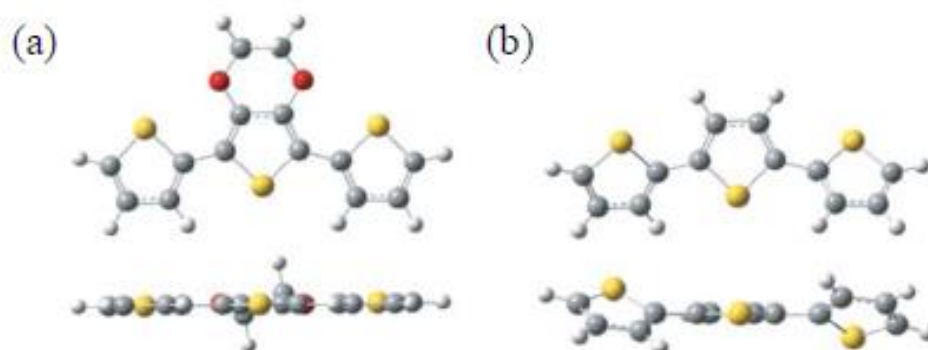


Fig. 4.2 Molecular structures of (a) **E3T** and (b) **3T** estimated by *ab initio* MO method (Gaussian09), HF/6-31G*, C_2 -symmetry.

4.3.3 Optical Properties of *EnTs*.

Electronic absorption spectra of other oligothiophenes, **E6T**, **E7T**, **E9T** and **E11T** are shown in Fig. 4.3. In all cases, broad bands with vibronic structure were observed

similarly to **E3T**. Although the bands showed a red-shift with increasing the length of oligothiophene chains reflecting the expansion of π -conjugation systems, the absorption maximum of **E11T** was similar to that of **E9T** because the effective π -conjugation may be disturbed by the steric hindrance of the four alkyl chains introduced at β -positions of thiophene rings. Previously, we have synthesized soluble thiophene hexamer and decamer (**6T** and **10T**, Fig. 4.4) which do not contain EDOT units.^[37,38,44] Compared with them, the absorption bands of oligothiophenes containing EDOT were remarkably red-shifted due to the electron-donating effect of oxygen atoms of EDOT unit and the enhancement of coplanarity to expand the effective π -conjugation length.

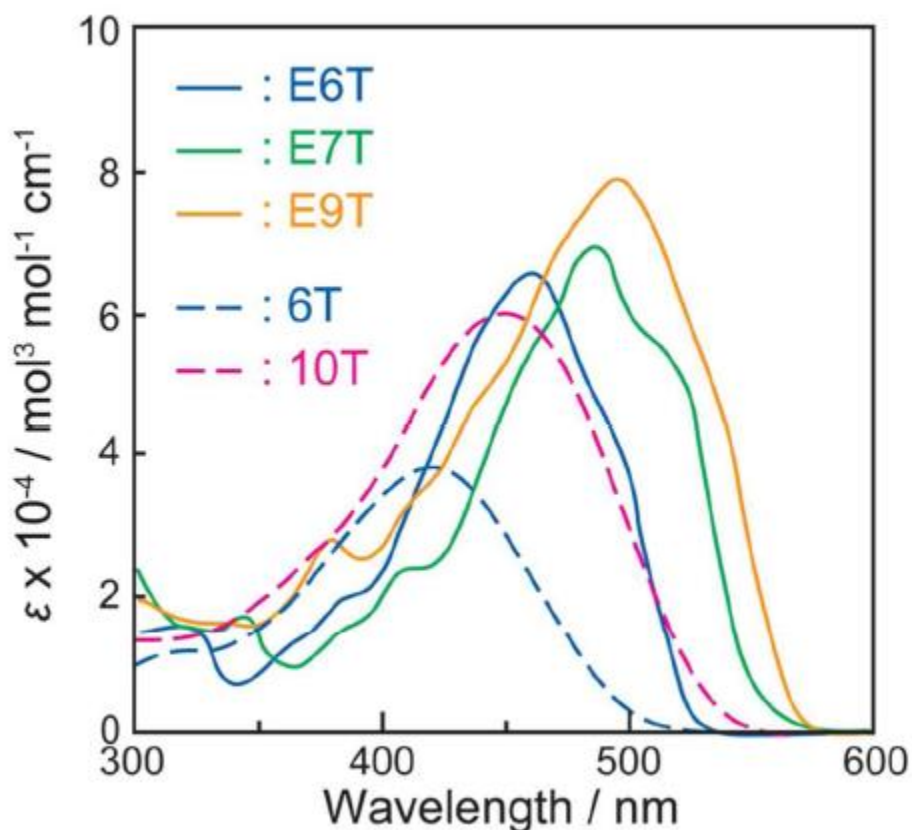


Fig. 4.3 Electronic absorption spectra of **EnTs** ($n = 6, 7, 9$ and 11) and **nTs** ($n = 6$ and 10) in dichloromethane solution.

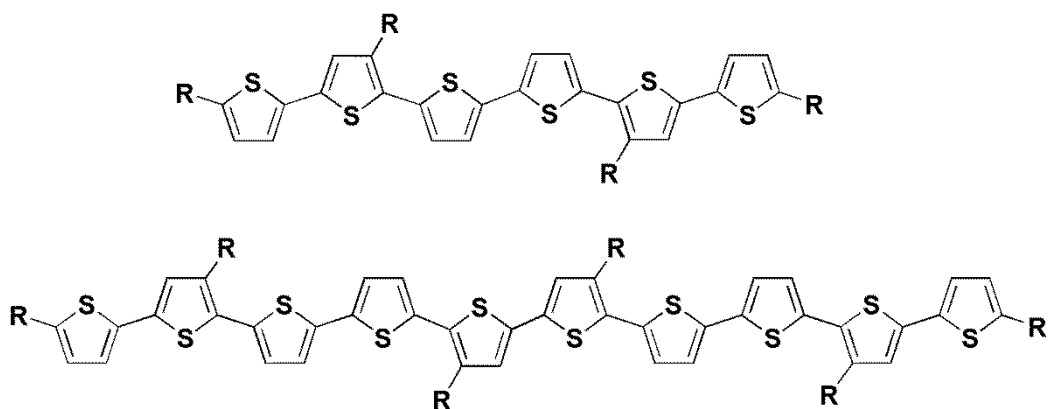


Fig. 4.4 Chemical structures of **6T** and **10T** (R = alkyl groups).

4.3.4 Electrochemical Stabilities of *EnT*.

Results of cyclic voltammeteries of *EnT*s are summarised in Table 1. **E3T** showed an oxidation peak at 0.50 V *vs.* Fc/Fc⁺, but the current of the corresponding reduction peak was very small. When the redox reaction was repeated, another oxidation peak was newly observed at around 0 V *vs.* Fc/Fc⁺, and the current of the redox peaks increased with increasing the number of redox cycles. We have already found that **E3T** can be electrochemically polymerized to form the polymer.^[31] Thus, this new peak can be ascribed to the redox reaction of the formed polymer. In the case of **E6T**, two redox reactions were observed at 0.08 and 0.57 V *vs.* Fc/Fc⁺. Among them, the first redox reaction was reversible, but the second one was irreversible and formed a polymeric material on the working electrode. **E7T** and **E9T** showed two reversible redox processes due to the stabilization of the formed charges by delocalization of π -electron systems. **E11T** showed broad peaks, but these peaks were found to contain two reversible redox processes from the spectroelectrochemical investigation.

Table 4.1 Redox potentials estimated from cyclic voltammetry^a

Oligothiophenes	E_{pa1} / V^b	E_{pc1} / V^b	E_{pa2} / V^b	E_{pc2} / V^b
E3T	0.50	ir ^c		
E6T	0.08	-0.05	0.57	ir ^c
E7T	-0.16	-0.36	0.33	ir ^c
E9T	-0.09	-0.26	0.40	0.13
E11T	br ^d	br ^d	br ^d	br ^d
6T	0.35	0.28	0.35	0.28
10T	0.20	0.13		

^a scan rate: 50 mV/sec, electrolyte: Bu₄NClO₄ (0.1M), solvent: CH₂Cl₂

^b vs. Fc/Fc⁺,

^c ir = irreversible,

^d br = broad peaks

4.3.5 Film Forming Property

For the application of **EnTs** to solid state devices such as transparent conductive films and field-effect transistors, we tried to fabricate thin films of **EnTs** by casting and/or spin-coating techniques. When the spin-coatings of **E3T**, **E6T**, **E7T** and **E9T** were tried onto substrates of SiO₂, ITO and OTS-modified SiO₂/Si, smooth and homogeneous films were not obtained. A plausible reason may be that these oligothiophenes are highly crystalline. Previously, we successfully obtained smooth films of 15 oligothiophenes combined with electrically inert polymer backbones, for

example, polyethylenes having pendant oligothiophenes,^[4,45-47] linear polymers including oligothiophene bridged by alkylenes or silylenes,^[48-51] and polysilsesquioxanes having oligothiophenes.^[32,37,38,44,52] Thus, smooth films of **EnTs** will be obtained by the introduction of inert polymer backbones, which is under investigation. We also tried to fabricate the film of **E7T** by a drop-cast method and found a unique morphology as shown in Fig. 4.5, where hexagonally ordered protuberances were observed. The mechanism is currently under investigation. On the other hand, smooth films of **E11T** were successfully obtained by a spin-coating method with a chloroform solution of **E11T** (10 mg/mL).

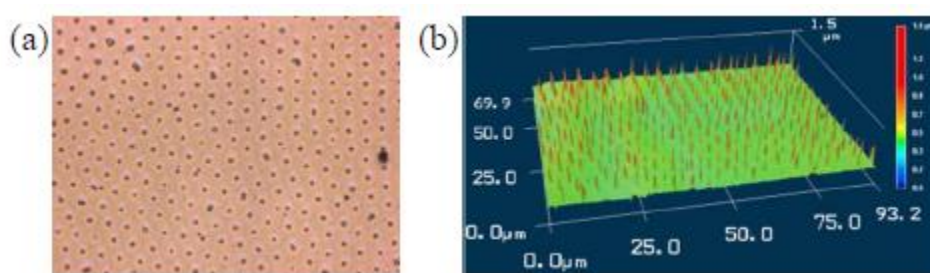


Fig. 4.5 Laser microscopic images of **E7T** film obtained by drop30cast method. (a) 2D and (b) 3D images.

4.3.6 Electrical Properties of Solid-state **E11T**.

Since smooth and thin films of **E11T** were obtained on SiO₂, ITO, and OTS-modified SiO₂/Si substrates, electrochemical and electrical properties of **E11T** films could be investigated.

Absorption spectra of **E11T** films biased at different potentials were measured in TEAP (0.1 M)–acetonitrile to identify chemical species formed at different oxidation

states (Fig. 4.6). At the neutral state, **E11T** showed only one sharp peak at around 500 nm due to a π - π^* transition. When the **E11T** was oxidized at 0.0 V vs. Ag/Ag^+ , two peaks were observed at around 700 and 1500 nm, and they were ascribed to the one-electron oxidized species of **E11T**. The intensity of these peaks increased with increasing the electrode potential, and reached a maximum at 0.3 V. When the **E11T** was oxidized at higher potentials than 0.3 V, the intensity of these peaks decreased and one broad peak due to the twoelectron oxidized species of **E11T** was newly observed at 1200 nm. These results suggest that **E11T** can be one- and twoelectron oxidized in the potential range from 0 to 0.8 V vs. Ag/Ag^+ . These spectral changes were reversible due to the electrochemical stability, and **E11T** showed the excellent electrochromic behaviour (Fig. 4.7).

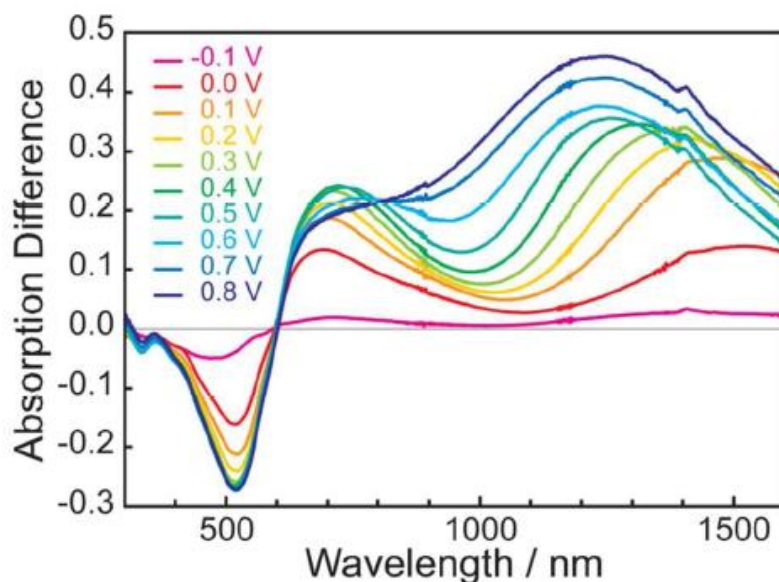


Fig. 4.6 Spectroelectrochemistry of **E11T** film.

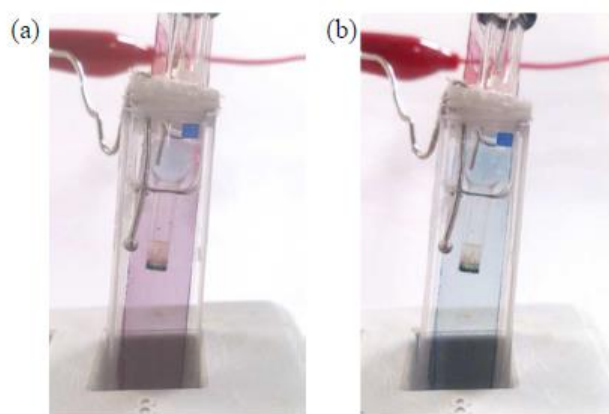


Fig. 4.7 Electrochromic behaviour of **E11T** film. (a) neutral and (b) oxidized films.

Fig.4.8 depicts semilogarithmic plots of doping level and conductivity against potential for **E11T**. In concert with the electrochemical oxidation, the doping level gradually increased and finally reached around 20% at 0.75 V. This value corresponds to 200% doping per **E11T**, suggesting that **E11T** is almost completely two-electron oxidized, which is consistent with the results of above-mentioned spectroelectrochemistry (Fig. 4.6). The electrical conductivities also increased with the increase in potential, but showed a maximum at 0.55 V vs. Ag/Ag⁺. The maximum value of doped **E11T** was 0.73 S cm⁻¹, which is slightly higher than that of dodecathiophene without EDOT (0.4 S cm⁻¹).^[37,38] This result indicates that the introduction of EDOT enhances the charge transport properties of oligothiophenes due to the stabilization of introduced positive charges.

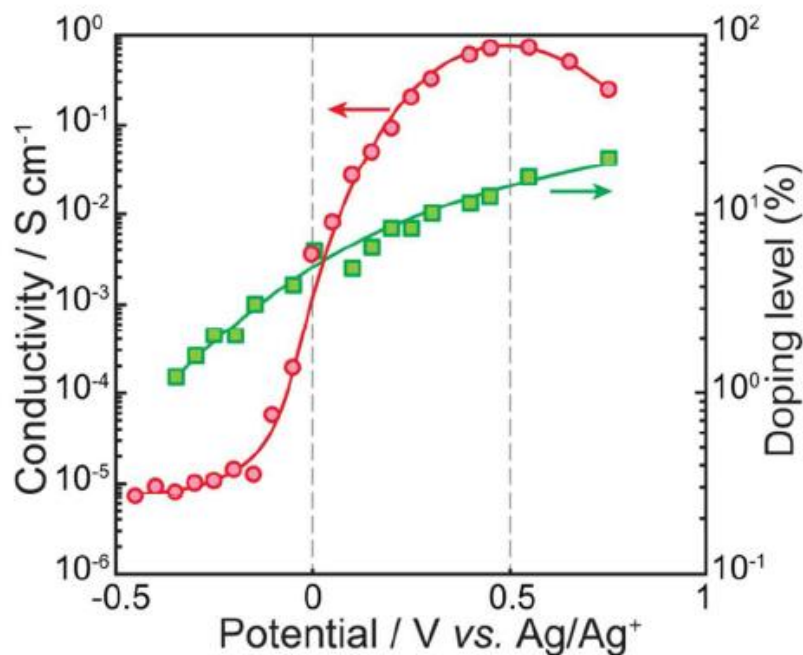


Fig. 4.8 Doping level and electrical conductivity of **E11T** film plotted against electrode potential.

To get an insight into transport properties of the **E11T**, apparent mobilities of charge carriers were estimated by combining doping level and conductivity data. The mobilities are plotted in Fig. 4.9 as a function of doping level. The mobilities at low doping levels below 3 % are $4^{-7} \times 10^{-7} \text{ cm}^2 \text{ V}^{-1} \text{ s}^{-1}$, which can be explained by the interchain hopping transport of monocation radicals (polarons).^[50,51] The mobility plots showed a maximum at a doping level of 13 %, in which one- and two-electron oxidized states coexist. When the doping level was increased beyond 15 %, the mobility slightly decreased. A plausible reason for this difference may be explained as follows: almost all **E11T** was two-electron oxidized at a doping level of 20 %, so that it becomes difficult for the positive charge to move because of a Coulombic repulsion. This result was observed in the oligothiophenes having silsesquioxane networks.^[32,37,38]

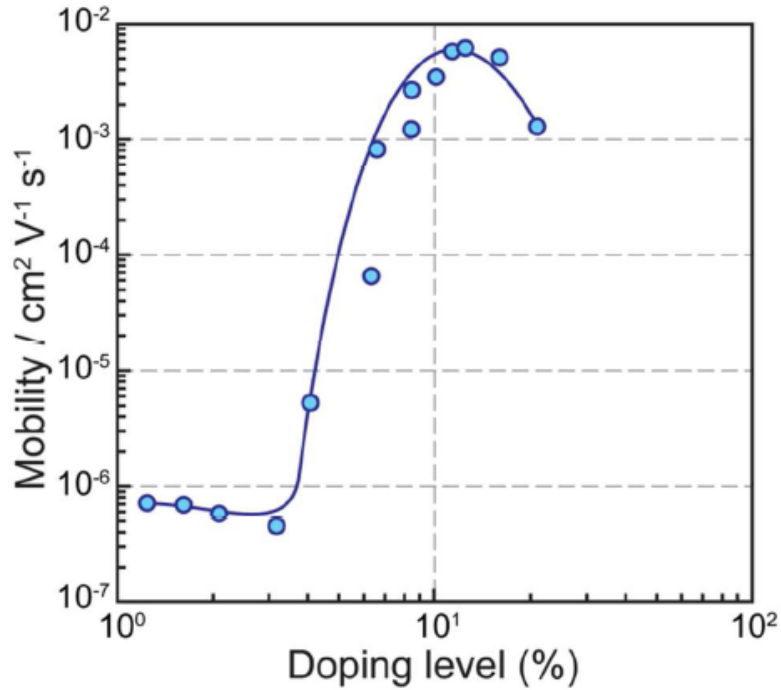


Fig. 4.9 Apparent mobilities of charge carriers in **E11T** film plotted against doping level.

Since **E11T** was found to have the good electrical conductivity from the experiment of *in-situ* conductivity measurement, it was expected that the field-effect transistor (FET) using **E11T** as a semiconducting layer will show a good performance. To confirm it, FET devices using **E11T** were preliminarily fabricated with different device preparation conditions and measured in Ar and air atmospheres (Table 4.2). Among them, the device using **E11T** film prepared on OTS-modified SiO₂/Si substrate by spin-coating with 3000 rpm showed the highest mobilities (3.4×10^{-4} and 6.6×10^{-4} cm² V⁻¹ s⁻¹ in Ar and air, respectively). Also, the device measured in Ar showed the better *I*_{on}/*I*_{off} ratio, because **E11T** will be oxidized in air. For the improvement of FET performances, the optimization of device fabrication is under investigation.

Table 4.2. Performances of FET using **E11T**.

Run	Rotational Speed ^a / rpm	SAM	Atmosphere ^b	μ FET / cm ² V ⁻¹ S ⁻¹	Ion/Ioff
1	2000	none	air	3.5×10^{-5}	4
2			Ar	4.3×10^{-5}	10
3		OTS	air	6.6×10^{-4}	9
4			Ar	3.4×10^{-4}	24
5	3000	none	air	- ^c	- ^c
6			Ar	1.3×10^{-5}	4
7		OTS	air	3.9×10^{-4}	8
8			Ar	1.2×10^{-4}	33

^a rotational speed of spin-coating for preparation of **E11T** film ^b measurement atmosphere, ^c not measured.

4.4 Conclusions

EDOT-containing oligothiophenes were newly synthesized and their optical and electrochemical properties were investigated. It was found that the introduction of EDOT caused the remarkable red-shift of absorption bands. Oxidation potentials were controlled by the introduction of EDOT and the length of oligothiophene chains. **E11T** showed good solubility in common organic solvents and could form smooth films by spin-coating. The electrical conductivity of electrochemically doped **E11T** was found to be higher than that of oligothiophene without EDOT and comparable to that of polythiophene.

4.5 References

1. A. Elschner, S. Kirchmeyer, W. Lovenich, U. Merker, and K. Reuter, *PEDOT Principles and Applications of an Intrinsically Conductive Polymer*, Boca Raton, CRC Press, 2011.
2. S. Kirchmeyer, and K. Reuter, *J. Mater. Chem.*, 2005, **15**, 2077.
3. A. Menon, H. Dong, Z. I. Niazimbetova, L. J. Rothberg, and M. E. Galvin, *Chem. Mater.*, 2002, **14**, 3668.
4. K. Nawa, K. Miyawaki, I. Imae, N. Noma, and Y. Shirota, *J. Mater. Chem.*, 1993, **3**, 113.
5. P. Bauerle, *Adv. Mater.*, 1992, **4**, 102.
6. P. Bauerle, *Oligothiophenes*. In: K. Mullen, and G. Wegner, editors. *Electronic materials: the oligomer approach*. Weinheim: Wiley-VCH; 1998.
7. R. D. McCullough, *Adv. Mater.*, 1998, **10**, 93.
8. J. Roncali, *J. Mater. Chem.*, 1999, **9**, 1875.
9. D. Fichou, *J. Mater. Chem.*, 2000, **10**, 571.
10. T. Otsubo, Y. Aso, and K. Takimiya, *Bull. Chem. Soc. Jpn.*, 2001, **74**, 1789.
11. M. R. Alves, H. D. R. Calado, T. Matencio, and C.L. Donnici, *Quim. Nova*, 2010, **33**, 2165.
12. A. Operamolla, and G. M. Farinola, *Eur. J. Org. Chem.*, 2011, **2011**, 423.
13. D. Fichou, *Handbook of oligo- and polythiophenes*. Weinheim: Wiley-VCH; 1999.
14. I. F. Perepichka, and D. F. Perepicjka, editors, *Handbook of thiophene-based*

materials: applications in organic electronics and photonics. Chichester: John Wiley & Sons Ltd; 2009.

15. J. L. Segura, and N. Martin, *J. Mater. Chem.*, 2000, **10**, 2403.
16. T. Otsubo, Y. Aso, and K. Takimiya, *J. Mater. Chem.*, 2002, **12**, 2565.
17. A. R. Murphy, and J. M. J. Frechet, *Chem. Rev.*, 2007, **107**, 1066.
18. A. Mishra, C. Q. Ma and P. Bauerle, *Chem. Rev.*, 2009, **109**, 1141.
19. Y. Aso, *Kobunshi*, 2009, **58**, 801.
20. J. L. Segura, H. Herrera, and P. Bauerle, *J. Mater. Chem.*, 2012, **22**, 8717.
21. G. A. Sotzing, J. R. Reynolds, and P. I. Steel, *Adv. Mater.*, 1997, **9**, 795.
22. S. Akoudad, and J. Roncali, *Synth. Met.*, 1998, **93**, 111.
23. G. A. Sotzing, J. R. Reynolds, and P. J. Steel, *Chem. Mater.*, 1996, **8**, 882.
24. M. P. de Jong, A. W. Denier van der Gon, X. Crispin, W. Osikowicz, W. R. Salaneck, and L. Groenendaal, *J. Chem. Phys.*, 2003, **118**, 6495.
25. J. J. Apperloo, L. "Bert" Groenendaal, H. Verheyen, M. Jayakannan, R. A. J. Janssen, A. Dkhissi, D. Beljonne, R. Lazzaroni and J.-L. Bredas, *Chem. Eur. J.*, 2002, **8**, 2384.
26. M. Turbiez, P. Frere and J. Roncali, *J. Org. Chem.*, 2003, **68**, 5357.
27. D. Wasserberg, S. C. J. Meskers, R. A. Janssen, E. Mena-Osteritz, and P. Bauerle, *J. Am. Chem. Soc.*, 2006, **128**, 17007.
28. R. G. Hicks, and M. B. Nodwell, *J. Am. Chem. Soc.*, 2000, **122**, 6746.
29. M. Turbiez, P. Frere, M. Allain, C. Videlot, J. Ackermann, and J. Roncali *Chem. Eur. J.*, 2005, **11**, 3742.
30. K. M. Nalin de Silva, E. Hwang, W. K. Serem, F. R. Fronczek, J. C. Garno, and E. E. Nesterov, *ACS Appl. Mater. Int.*, 2012, **4**, 5430.

31. I. Imae, S. Imabayashi, K. Korai, T. Mashima, Y. Ooyama, K. Komaguchi, and Y. Harima, *Mater. Chem. Phys.*, 2012, **131**, 752.
32. I. Imae, D. Tokita, Y. Ooyama, K. Komaguchi, J. Ohshita, and Y. Harima, *Polym. Chem.*, 2011, **2**, 868.
33. Y. Harima, T. Eguchi, and K. Yamashita, *Synth. Met.*, 1998, **95**, 69.
34. Y. Harima, T. Eguchi, K. Yamashita, K. Kojima, and M. Shiotani, *Synth. Met.*, 1999, **105**, 121.
35. Y. Harima, Y. Kunugi, K. Yamashita, and M. Shiotani, *Chem. Phys. Lett.*, 2000, **317**, 310.
36. H. Tang, L. Zhu, Y. Harima, and K. Yamashita, *Synth. Met.*, 2000, **110**, 105.
37. I. Imae, D. Tokita, Y. Ooyama, K. Komaguchi, J. Ohshita, and Y. Harima, *J. Mater. Chem.*, 2012, **22**, 16407.
38. I. Imae, S. Takayama, D. Tokita, Y. Ooyama, K. Komaguchi, J. Ohshita, and Y. Harima, *Int. J. Polym. Sci.*, 2012, **2012**, 484523.
39. J.-M. Raimundo, P. Blanchard, P. Frere, N. Mercier, I. Ledoux-Rak, R. Hierle, and J. Roncali, *Tetrahedron Lett.*, 2001, **42**, 1507.
40. P. Leriche, M. Turbiez, V. Monroche, P. Frere, P. Blanchard, P. J. Skabarab, and J. Roncali, *Tetrahedron Lett.*, 2003, **44**, 649.
41. S. S. Zade, S. Panda, H. B. Singh, R. B. Sunoj, and R. J. Butcher, *J. Org. Chem.*, 2005, **70**, 3693.
42. D. Roy, and R. B. Sunoj, *J. Phys. Chem. A*, 2006, **110**, 5942.
43. T. Ozaki, A. Nomoto, and A. Ogawa, *Heteroatom. Chem.*, 2011, **22**, 579.
44. Y. Harima, J. Ohshita, I. Imae, T. Sugioka, and K. Kanehira, *Jpn. Kokai Tokkyo Koho*, 2010, 266727.

45. K. Nawa, I. Imae, N. Noma, and Y. Shirota, *Macromolecules*, 1995, **28**, 723.
46. I. Imae, K. Nawa, Y. Ohsedo, N. Noma, and Y. Shirota, *Macromolecules*, 1997, **30**, 380.
47. Y. Ohsedo, I. Imae, and Y. Shirota, *J. Polym. Sci., Pt. B*, 2003, **41**, 2471.
48. X. Jiang, Y. Harima, L. Zhu, Y. Kunugi, K. Yamashita, M. Sakamoto, and M. Sato, *J. Mater. Chem.*, 2001, **11**, 3043.
49. X. Jiang, Y. Harima, K. Yamashita, A. Naka, K. K. Lee, and M. Ishikawa, *J. Mater. Chem.*, 2003, **13**, 785.
50. Y. Harima, X. Jiang, Y. Kunugi, K. Yamashita, A. Naka, K. K. Lee, and M. Ishikawa, *J. Mater. Chem.*, 2003, **13**, 1298.
51. Y. Harima, D.-H. Kim, Y. Tsutitori, X. Jiang, R. Patil, Y. Ooyama, J. Ohshita, and A. Kunai, *Chem. Phys. Lett.*, 2006, **420**, 387.
52. I. Imae, S. Takayama, D. Tokita, Y. Ooyama, K. Komaguchi, J. Ohshita, T. Sugioka, K. Kanehira, and Y. Harima, *Polymer*, 2009, **50**, 6198.

Chapter 5

Summary

My research attention was paid to the conductive polymers and oligomers. In this thesis, I describe the synthesis of novel π -conjugated oligomers and D-A type copolymers for optoelectronic applications. The main contents of this thesis were arranged as follow.

- ◆ The background of the organic semiconductors was introduced generally.
- ◆ **PM1** and **PM2** are synthesized. The main-chain type polymers show a good thermal stability and a broad absorption band. Slight difference of the properties between the two polymers may be caused by the length of the alkoxy group. The D-A type polymers with proper D unit and A unit are the potential materials for photovoltaic applications.
- ◆ **PS0**(without conjugated side chain), **PS1**(with conjugated side-chain), and **PS2**(with conjugated side chain containing an electron-deficient group) were synthesized. In the case of **PS2**, the light harvesting ability, energy levels and photovoltaic properties is better than those of other

two polymers. The results reveal that the introduction of the conjugated side-chain with an electron-deficient group to a polymer backbone is an effective approach for improving the photovoltaic materials.

- ◆ Five oligothiophenes (*EnTs*, $n=3,6,7,9,11$) with EDOT were synthesized. The EDOT unit induced a red shift of absorption bands and a negative shift of oxidation potentials. The E11T showed a conductivity of 1 S/cm. A FET device based on E11T showed the highest mobilities (3.4×10^{-4} and $6.6 \times 10^{-4} \text{ cm}^2 \text{ V}^{-1} \text{ s}^{-1}$ in Ar and air. The pendent unit is important to tuning the properties of materials.

Acknowledgement

I would like to acknowledge Hiroshima University, and the Graduate school of Engineering for providing me a chance and a favorable academic circumstance for my study in Hiroshima University.

I am very grateful for the China Scholarship Council and the Ministry of Education of the P. R. China for providing me the State Scholarship.

I would express my heartiest gratitude to my reverend supervisors, Professor Yutaka Harima and Dr. Ichiro Imae. It is great honor for me to have done my research work under their supervision. Their intellectual guidance and kind encouragement make my research and daily life very smooth. Any progress in the course of my research will be impossible if without their full instruction. I would say thanks to Professor Joji Ohshita for his genuine interest and assistance in my research. Very gratefully I acknowledge Dr. Kenji Komaguchi and Dr. Yousuke Ooyama for sacrificing their valuable time and special talent about my research.

I also thank all the other members of Professor Yutaka Harima's laboratory for their great help. Great thanks to all the members in the office of the Division of Applied Chemistry.

I would like to thank Professor Yutaka Harima, Professor Joji Ohshita, Dr. Ichiro Imae, Dr. Yousuke Ooyama, and Dr. Kenji Komaguchi for their reviewing my doctoral thesis with important comments and suggestions.

My sincere thanks are due to all of my friends and well wishes to who helped me in

various ways throughout my stay in Japan.

Finally, I would like to give my heartiest thanks to my wife Xiaoxue Ye and my lovely family for their continuous encouragement and mental support, without which it would not have been possible to come this far in my studies.

List of related publications

1. Zhifang Tan, Ichiro Imae, Yousuke Ooyama, Kenji Komaguchi, Joji Ohshita, Yutaka Harima. Low Bandgap Polymers with Benzodithiophene and Bisthienylacrylonitrile Units for Photovoltaic Applications. *European Polymer Journal*, 2013, **49**, 1634-1641.
2. Zhifang Tan, Ichiro Imae, Kenji Komaguchi, Yousuke Ooyama, Joji Ohshita and Yutaka Harima. Effects of π -conjugated side chains on properties and performances of photovoltaic copolymers. *Synthetic Metals*, 2014, **187**, 30-36
3. Ichiro Imae, Saki Imabayashi, Kenji Komaguchi, Zhifang Tan, Yousuke Ooyama and Yutaka Harima, Synthesis and Electrical Properties of Novel Oligothiophenes Partially Containing 3,4-Ethylenedioxythiophenes. *RSC Advances*, 2014, **4**, 2501-2508.